CELLULAR NEUROSCIENCE

CHI3L1 signaling impairs hippocampal neurogenesis and cognitive function in autoimmune-mediated neuroinflammation

Wei Jiang[1]†, Fan Zhu[1]†, Huiming Xu[1]†, Li Xu[1], Haoyang Li[1], Xin Yang[2], Shabbir Khan Afridi[3], Shuiqing Lai[4], Xiusheng Qiu[5], Chunxin Liu[1], Huilu Li[6], Youming Long[6], Yuge Wang[1], Kevin Connolly[2], Jack A. Elias[2], Chun Geun Lee[2], Yaxiong Cui[7]*, Yu-Wen Alvin Huang[2,8]*, Wei Qiu[1]*, Changyong Tang[1]*

Chitinase-3–like protein 1 (CHI3L1) is primarily secreted by activated astrocytes in the brain and is known as a reliable biomarker for inflammatory central nervous system (CNS) conditions such as neurodegeneration and autoimmune disorders like neuromyelitis optica (NMO). NMO is an astrocyte disease caused by autoantibodies targeting the astroglial protein aquaporin 4 (AQP4) and leads to vision loss, motor deficits, and cognitive decline. In this study examining CHI3L1's biological function in neuroinflammation, we found that CHI3L1 expression correlates with cognitive impairment in our NMO patient cohort. Activated astrocytes secrete CHI3L1 in response to AQP4 autoantibodies, and this inhibits the proliferation and neuronal differentiation of neural stem cells. Mouse models showed decreased hippocampal neurogenesis and impaired learning behaviors, which could be rescued by depleting CHI3L1 in astrocytes. The molecular mechanism involves CHI3L1 engaging the CRTH2 receptor and dampening β-catenin signaling for neurogenesis. Blocking this CHI3L1/CRTH2/β-catenin cascade restores neurogenesis and improves cognitive deficits, suggesting the potential for therapeutic development in neuroinflammatory disorders.

INTRODUCTION

Chitinase-3–like protein 1 (CHI3L1; also known as YKL-40 in humans and BMP-39 in mice) is a secreted glycoprotein that belongs to the diverse glycoside hydrolase family 18 (*1*–*3*). In circulation and peripheral tissues, our collaborative group and others have documented that CHI3L1 functions as a signaling molecule to mediate a wide range of immune and inflammatory responses by engaging a defined set of surface receptors and downstream signaling cascades (*4*–*10*). In the brain, the limited yet emerging literature demonstrates that CHI3L1 is primarily secreted by activated astrocytes and indicates a neurotoxic inflammatory state of neuroinflammation (*2*, *11*–*13*). CHI3L1 is a high-profile biomarker for an array of neurological disorders hallmarked by neuroinflammation, including the neurodegenerative condition of Alzheimer's disease (*14*, *15*), the malignancy of glioblastoma (*13*, *16*), and autoimmune disorders such as multiple sclerosis (*17*) and neuromyelitis optica (NMO) spectrum disorder (*18*–*20*). To date, little is known about the biological role of this astroglial factor CHI3L1 in neuroinflammation and CNS disease manifestations.

Being a well-characterized astrocyte disease, NMO is an uncommon disabling autoimmune central nervous system (CNS) disorder resulting from the primary astrocytopathy caused by autoantibodies targeting the astroglial surface protein aquaporin 4 (AQP4), which serves as the major diagnostic criterion (*21*). Secondary to the AQP4 immunoglobulin G (IgG)–induced astroglial activation, the demyelination and neuronal damage manifest as relentless loss of spinal cord and optic nerve functions, as well as salient cognitive impairment that greatly aggravates the disease burden (*22*, *23*). Of note, anatomical and functional abnormalities of the hippocampus have been reported in clinical studies of NMO by us and others, corroborating the structural basis of hippocampal dysfunction in astroglial activation (*24*–*28*). Given the strong correlation between the CHI3L1 level and clinical severity in NMO (*18*–*20*), it is thus of our high interest to investigate the involvement of CHI3L1 in the development of hippocampal dysfunction and cognitive impairment in neuroinflammation.

Within the hippocampus, one well-defined cell type has been independently validated to be affected by neuroinflammatory responses—the neural stem cells (NSCs). Scores of studies solidly described the noxious effects of neuroinflammation on the proliferation and neuronal differentiation of NSCs—the process of neurogenesis—in the hippocampus subgranular zone (SGZ) from adult mouse brains (*29*–*31*). The inflammatory cytokines and other factors secreted by activated glia in the microenvironment have been shown to account for such inhibitory effects (*29*–*32*).

[1]Department of Neurology, The Third Affiliated Hospital of Sun Yat-sen University, 600 Tianhe Road, Guangzhou, Guangdong Province 510630, China. [2]Department of Molecular Biology, Cell Biology, and Biochemistry, Brown University, 70 Ship Street, Providence, RI 02903, USA. [3]Faculty of Biological Sciences, School of Biomedical Sciences, University of Leeds, Leeds LS2 9JT, UK. [4]Department of Endocrinology, Guangdong Provincial People's Hospital, Guangdong Academy of Medical Sciences, 106 Zhongshan Er Road, Guangzhou, Guangdong Province 510080, China. [5]Vaccine Research Institute, The Third Affiliated Hospital of Sun Yat-sen University, 600 Tianhe Road, Guangzhou, Guangdong Province 510630, China. [6]Department of Neurology, The Second Affiliated Hospital of Guangzhou Medical University, 250 Changgang East Road, Guangzhou, Guangdong Province 510260, China. [7]State Key Laboratory of Membrane Biology, Tsinghua-Peking Center for Life Sciences, IDG/McGovern Institute for Brain Research, Beijing Advanced Innovation Center for Structural Biology, School of Pharmaceutical Sciences, Tsinghua University, Beijing 100084, China. [8]Center for Translational Neuroscience, Carney Institute for Brain Science, Brown University, 70 Ship Street, Providence, RI 02903, USA.
*Corresponding author. Email: tangchy23@mail.sysu.edu.cn (C.T.); qiuwei120@vip.163.com (W.Q.); alvinhuang@brown.edu (Y.-W.A.H.); cuimarcus@mail.tsinghua.edu.cn (Y.C.)
†These authors contributed equally to this work.

Prompted by our prior studies on NSC differentiation and inflammatory signaling mechanism (*33*–*35*), we decided to focus on NSCs and aimed at illustrating a distinct cellular signaling mechanism of CHI3L1 as the proof of concept for a fundamental CHI3L1 function in the brain.

In this study, we first confirmed the induction of CHI3L1 and neuroinflammatory features in cultured astrocytes activated by well-characterized proinflammatory stimuli, including the cytokine interleukin-1β (IL-1β) and AQP4 autoantibodies. CHI3L1 secreted from the activated astrocytes drastically inhibited NSC proliferation and neuronal differentiation in vitro. In vivo, we analyzed hippocampal tissues from young adult mice overexpressing CHI3L1 or receiving the passive transfer of anti-AQP4 IgG (*36*–*39*) that activated astrocytes to induce CHI3L1 secretion and triggered neuroinflammation. We noted a significant reduction in adult hippocampal neurogenesis and defective learning behaviors. Notably, such in vivo defects can be rescued by CHI3L1 depletion in astrocytes. We sought to define the signaling mechanism whereby CHI3L1 governs the detrimental effect on neurogenesis by identifying the receptor and downstream pathway in NSCs. Mechanistically, CHI3L1 engages the CRTH2 receptor and dampens β-catenin signaling, which is critical for neurogenesis. Last, we showed that this CHI3L1/CRTH2/β-catenin cascade can be targeted to restore neurogenesis and ameliorate cognitive deficits resulting from neuroinflammation. Our findings provide pioneering evidence for the biological role of CHI3L1 in the brain, departing from its long-regarded role as merely a biomarker. The discoveries we made here would be highly advantageous for the development of much-needed therapeutics to prevent neuroinflammatory toxicity going beyond NMO and relevant autoimmune brain diseases.

RESULTS

CHI3L1 is induced in astrocytes activated by proinflammatory stimuli of cytokines and antibody-mediated immune response

We first confirmed the induction of CHI3L1 in activated astrocytes by analyzing two independent transcriptome datasets of mouse astrocytes undergoing neurotoxic activation after inflammatory stimulation in vivo (*40*) and in vitro (*41*). In astrocytes acutely purified from young adult mice subject to intraperitoneal injection of lipopolysaccharide (LPS), the CHI3L1 level was dramatically increased [fig. S1A in vivo; Hasel *et al.* (*40*)]; the increase was even more obvious in the cultures of primary astrocytes treated with proinflammatory cytokines of IL-1, tumor necrosis factor (TNF), and C1q [ITC; fig. S1A in vitro; Guttenplan *et al.* (*41*)]. To further investigate the role of CHI3L1 in immune-mediated neuroinflammation, we prepared primary astrocyte cultures with high purity (fig. S1B) and functional maturity (fig. S1C) and treated them with IL-1β, monoclonal mouse antibodies against AQP4 (msAQP4-IgG) (*39*), and human anti-AQP4 autoantibodies purified from NMO patients′ plasma (hsAQP4-IgG) (*37*, *38*), with control conditions of vehicle [phosphate-buffered saline (PBS)], mouse control IgG (msCtrl-IgG), and human control IgG (hsCtrl-IgG, pooled from healthy subjects′ plasma), respectively (Fig. 1A). The binding of anti-AQP4 IgG to the surface AQP4 protein on astrocytes in vitro was repeatedly shown to provoke inflammatory features (*36*–*38*) and, more importantly, to internalize and degrade AQP4 in astrocytes—a distinctive pathology hallmark that distinguishes NMO from the relevant autoimmune disease multiple sclerosis (*21*). We observed marked induction of CHI3L1 mRNA level in all three treatment conditions by quantitative real-time polymerase chain reaction (qPCR) assays, with the hsAQP4-IgG being the most robust one (Fig. 1B). All three treatments also caused a surge in protein levels of CHI3L1 and glial fibrillary acidic protein (GFAP), signifying the activation of astrocytes (Fig. 1, C and D). Only the treatments with anti-AQP4 antibodies (Fig. 1D), but not IL-1β (Fig. 1C), led to the loss of AQP4 expression. To systemically probe the cellular consequences of immune-mediated astroglial activation, we referred to prior studies based on the use of human IgG derived from NMO patients (*37*, *38*) and RNA-sequenced mouse astrocytes nontreated or treated with three independent replicate batches of our hsAQP4-IgG or hsCtrl-IgG. Overall, we noticed a considerable change in gene profile that distinctly separated the clusters of hsAQP4 and control IgG treatment samples (fig. S1D). We identified a total of 152 differentially expressed genes (DEGs) that met our statistical criteria, with 110 up-regulated and 42 down-regulated ones (fig. S1E and Fig. 1, E and F). The gene ontology (GO) enrichment analysis showed a clear picture of inflammatory and immunological responses (fig. S1F). The induction of a reactive program was further corroborated after we contrasted our data with a similar astroglial transcriptome dataset from Walker-Caulfield *et al.* (*37*) based on array-based gene expression analysis. The overlap of 91 genes out of our 152 DEGs was considerable (Fig. 1, E and F), and the hierarchical clustering of the heatmap based on these 91 overlapped DEGs clearly discerned the hsCtrl-IgG and hsAQP4-IgG samples and depicted the transcriptional signature of immune-mediated astroglial activation (Fig. 1E). The most significantly enriched GO pathways for these overlapped genes (Fig. 1G) were akin to the analysis of our own DEGs (fig. S1F) and included cellular responses to proinflammatory cytokines and viral infections. The 21 secreted proteins that overlapped between the two studies outlined the core response of immune-activated astrocytes, with CHI3L1 as a key responder (Fig. 1H). We integrated the data from our untreated samples to discriminate the effect from hsCtrl-IgG treatment and pinpointed the GO pathway of neuroinflammation. We recognized a group of C—C and C—X—C motif chemokine genes, including CCL2, CCL5, CCL6, CCL7, CCL17, CXCL1, and CXCL10, together with IL-1α and IL-β that denoted the hsAQP4-IgG–induced neuroinflammatory feature (Fig. 1I). The analysis of the overlap by a published gene change pattern of astrocyte activation (*42*) revealed CHI3L1 as a top gene that distinguished the hsCtrl-IgG– and hsAQP4-IgG–treated astrocytes (Fig. 1J). In addition, we inquired into the analyses of the 91 overlapped DEGs for the involved cellular pathways by using two distinct computational tools: the Pathview (*43*) based on the Kyoto Encyclopedia of Genes and Genomes (KEGG) (*44*) and the Gene Set Enrichment Analysis (GSEA) (*45*). The nuclear factor κB (NFκB) canonical pathway—which has been documented to be critical for neurotoxic inflammation of astrocytes (*46*) and can be activated by CHI3L1 (*47*)—was the most prominent one in hsAQP4-IgG–induced astroglial activation (fig. S1, G and H). These findings jointly supported the notion that CHI3L1 is induced in astrocytes activated by immune-mediated inflammatory stimuli and is an important secreted protein in neuroinflammation associated with the astroglial autoimmune response of hsAQP4-IgG expression.

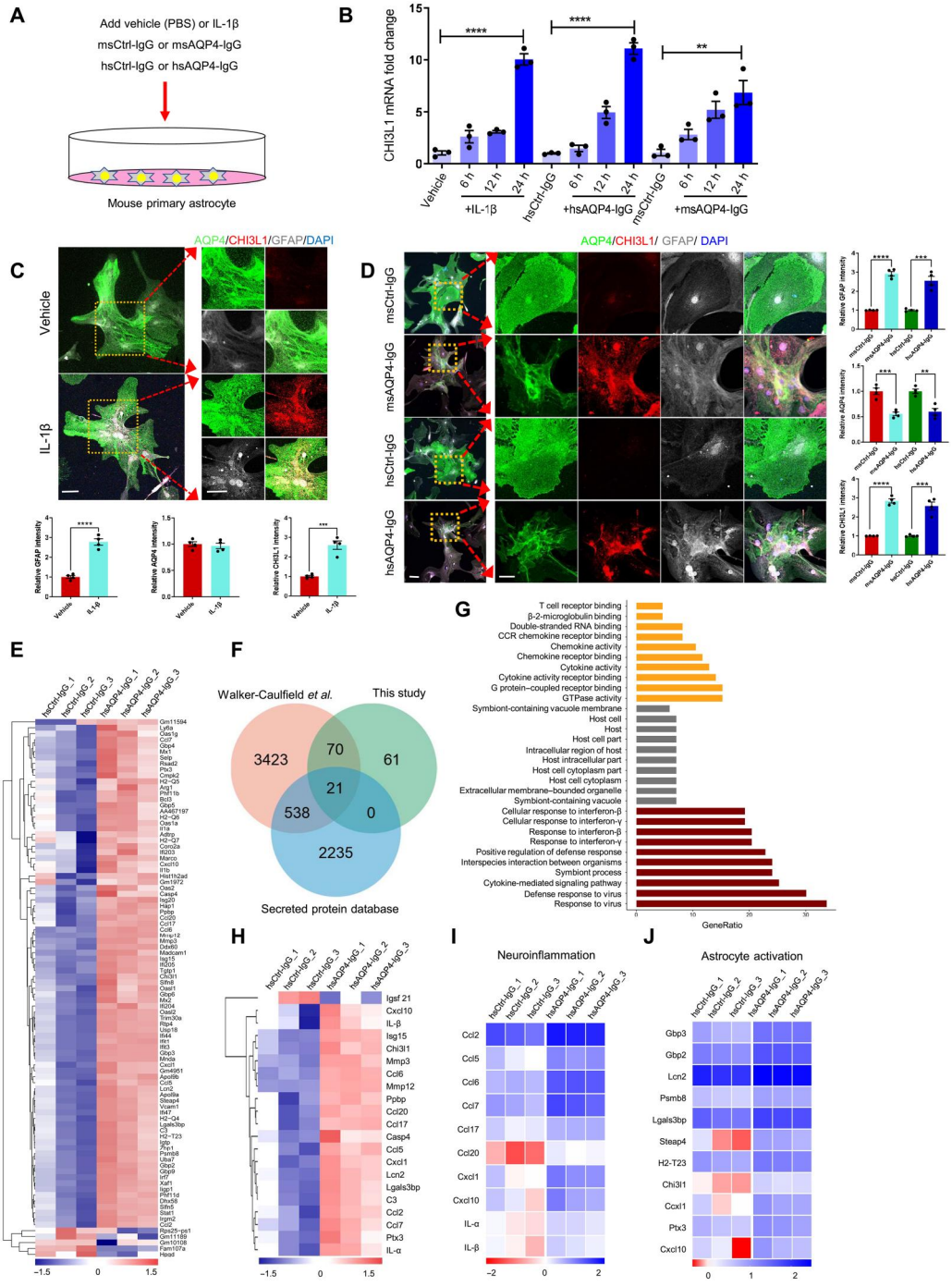

Fig. 1. Characterization of CHI3L1 induction and inflammatory features of primary astrocytes activated by the proinflammatory stimuli. (**A**) Schematic diagram showing the treatment of primary mouse astrocyte cultures with IL-1β (100 ng/ml) or PBS, the monoclonal mouse antibodies against AQP4 (msAQP4-IgG, 100 ng/ml) or the control mouse IgG (msCtrl-IgG, 100 ng/ml), and human anti-AQP4 autoantibodies purified from NMO patients (hsAQP4-IgG, 100 ng/ml) or control human IgG (hsCtrl-IgG, 100 ng/ml). (**B**) Relative levels of CHI3L1 mRNA in primary astrocytes treated with IL-1β, msAQP4-IgG, or hsAQP4-IgG. $n = 3$. (**C**) Representative images and quantification of astroglial marker expression in astrocyte cultures treated with PBS or IL-1β after 24 hours. $n = 4$. (**D**) Representative images and quantification of astroglial marker expression in astrocyte cultures treated with msAQP4-IgG or hsAQP4-IgG, alongside msCtrl-IgG or hsCtrl-IgG for 24 hours. $n = 4$. (**E**) RNA-seq of hsCtrl-IgG– and hsAQP4-IgG–treated astrocytes, with 91 DEGs being overlapped with the dataset of Walker-Caulfield *et al.* (*37*), shown in hierarchical clustering heatmap of gene fold changes (normalized to the untreated astrocytes). (**F**) Venn diagram of the overlapped DEGs in comparison to the genome-wide dataset of all secreted proteins. (**G**) GO enrichment analysis of the 91 overlapped DEGs. (**H**) Hierarchical clustering of 21 overlapped DEGs that were secreted proteins. (**I**) Analysis of the gene fold changes in the overlapped DEGs with the GO of neuroinflammation. (**J**) Analysis of the gene fold changes in the overlapped DEGs by the gene set of astrocyte activation [Zamanian *et al.* (*42*); "reactive"]. Scale bar, 100 μm. The bar graphs were presented as means ± SEM; the statistical evaluation of (C) and (D) was performed with Student's *t* test for two conditions; for (B), with one-way analysis of variance (ANOVA) and Tukey's post hoc multiple comparisons. $^{**}P < 0.01$, $^{***}P < 0.001$, $^{****}P < 0.0001$.

CHI3L1 secretion correlates with neurocognitive impairment and hippocampal dysfunction in human brains affected by autoimmune-mediated astrocyte activation

To investigate the clinical relevance of an elevated CHI3L1 level in neuroinflammation, we examined our multicenter, longitudinal NMO patient cohort with complete disease records, which is larger than all prior studies to date (*18*, *19*, *20*) and comprises 73 patients and 46 age-matched healthy controls (table S1). The autoantibodies against AQP4 were detected in all patients, and in agreement with all prior studies (*18*, *19*, *20*, *48*), the demographic data well reflected the dominance of young women (mean age: 42.8 ± 12.1 years; male/female = 7/66) and the high prevalence of brain demyelinating lesions, myelitis, and optic neuritis (table S2 and fig. S2A). We measured serum CHI3L1 levels in a subset of healthy controls and NMO patients, and noticed significantly higher values in the patient group (Fig. 2A and table S2; healthy controls: 25.2 ± 9.4 ng/ml, NMO: 47.7 ± 28.0 ng/ml). The measurements of cerebrospinal fluid (CSF) CHI3L1 levels also showed a significant increase in NMO patients, based on samples collected from another subset of this cohort (Fig. 2A and table S2; healthy controls: 95.5 ± 43.4 ng/ml, NMO: 143.8 ± 54.2 ng/ml). In addition, as we described earlier, we performed immunohistochemical examinations on biopsied live brain tissues from our prior study (*33*, *49*) including one NMO patient and one non-NMO control of head trauma patient (table S3). In addition to the characteristic reduction of AQP4 expression within the end-feet of astrocytes (along the vasculature labeled by endothelial marker CD31), we found that nearly all astrocytes (labeled with GFAP) were positive for CHI3L1 (Fig. 2B). Unique to our cohort is the comprehensive neuropsychological assessments, including the batteries of Hamilton Anxiety Rating Scale (HARS) and Hamilton Depression Rating Scale (HDRS) for general anxiety and depression-like symptoms, as well as the standard tests of Mini-Mental State Examination (MMSE), Symbol Digit Modalities Test (SDMT), Brief Visuospatial Memory Test Revised (BVMT-R), and five formats of California Verbal Learning Test (CVLT-LDFR, CVLT-SDCR, CVLT-SDFR, CVLT-LDCR, and CVLT-T1-5) for learning and memory-related performance. The difference between healthy controls and NMO patients was significant in all the assessments, substantiating the cognitive impairment that could be overshadowed by the neurological focal signs of motor and visual function losses (Fig. 2C and fig. S2, B and C). The neuropsychological disabilities documented here greatly correlated with the CHI3L1 serum levels in individual NMO patients. HARS and HDRS assessments corresponded positively with CHI3L1 levels and indicated the heightened mental stress reactions in response to the disease burden (Fig. 2C and fig. S2, B and C). We were much impressed by the potent negative correlation between the CHI3L1 level and the severity of learning and memory defects measured by MMSE, SDMT, BVMT-R, and all five subforms of CVLT (Fig. 2C). To emphasize the brain structural basis of the cognitive impairment associated with CHI3L1 expression in NMO, we carried out detailed analyses of the hippocampal regions based on the magnetic resonance imaging (MRI) scans (Fig. 2D). Consistent with case reports in the literature, our NMO patients had apparent volume atrophy of the hippocampus (Fig. 2, E and F), which was assigned as a biomarker for poor cognitive performance (*24*, *26*). Our additional analyses of hippocampal subregions (Fig. 2D) markedly expanded the imaging studies of NMO (fig. S2, D and E) and further highlight the hippocampal dysfunction in cognitive impairment potentially modulated by CHI3L1 in neuroinflammation.

Astrocyte-secreted CHI3L1 reduces proliferation and differentiation of NSCs in immune-mediated neuroinflammation

To test our hypothesis that CHI3L1 secreted by activated astrocytes contributes to the hippocampal dysfunction underlying the neuroinflammation-related cognitive impairment, we decided to focus on a specialized hippocampal cell type, the NSC, which is vital in maintaining proper size and function of the mammalian hippocampi and highly sensitive to inflammatory microenvironment (*29*–*31*). We thus purified and cultured primary mouse NSCs from the dissected dentate gyri of young adult wild-type mice (*50*) and differentiated these cells into neurons in vitro, with or without the treatment of recombinant CHI3L1 proteins (Fig. 2G), a method that our collaborative group and others have shown to well mimic the secretion of CHI3L1 by immune cells (*7*, *51*). Given that we showed earlier that multiple secretary proteins could be induced by hsAQP4-IgG (Fig. 1, F, I, and J), we also included the recombinant proteins of eight other identified astroglial factors to test their effects on NSC proliferation and neuronal differentiation. CHI3L1 was the only one that constantly exhibited inhibition on the process of neurogenesis in vitro (fig. S2, F and G). Specifically, the CHI3L1 treatment lowered the proliferation of NSCs by ~50% (Fig. 2H) and reduced the number of newborn neurons (Fig. 2I). To directly examine the effect of CHI3L1 secreted by immune-activated astrocytes on NSCs, we treated primary mouse astrocytes with hsCtrl-IgG or NMO patient–derived hsAQP4-IgG (Fig. 1D) and then harvested the astrocyte-conditioned media (ACM; Fig. 2J). The ACM from hsAQP4-IgG–treated astrocytes contained a higher level of secreted CHI3L1 (Fig. 2K). We sought to isolate CHI3L1 and determine its necessity by removing CHI3L1 with a monoclonal neutralizing antibody targeting against CHI3L1—an approach verified by our group and others to efficiently block the function of the secreted CHI3L1 *7* (*52*). As expected, ACM from hsAQP4-IgG–treated astrocytes diminished the NSC proliferation (Fig. 2, L and M) and differentiation into neurons (Fig. 2, N and O). The administration of the CHI3L1 neutralizing antibody abolished the inhibitory effect of the hsAQP4-IgG ACM on NSC proliferation and neuronal differentiation. These findings collectively suggested that CHI3L1 secreted by activated astrocytes impairs NSC proliferation and neurogenesis and precipitates hippocampal dysfunction and cognitive impairment.

Immune-mediated astrocytopathy impairs hippocampal neurogenesis and hippocampus-dependent learning behaviors in young adult mouse brains

Having shown that CHI3L1 secreted by immune-activated astrocytes reduced NSC proliferation and differentiation in vitro, we next pursued to determine whether the same effect could be observed in vivo. We followed and optimized the passive transfer method (*53*, *54*) to construct the mouse model of immune-mediated astrocytopathy as in NMO, via passive transfer of the control (msCtrl-IgG) or anti-AQP4 antibodies (msAQP4-IgG) (Fig. 1, B and D). We first stereotaxically injected the antibodies into the dentate gyri of 8-week-old wild-type mice on both sides (Fig. 3A, left). To assess the adult hippocampal neurogenesis, these injected mice then received pulse labeling of bromodeoxyuridine (BrdU) or

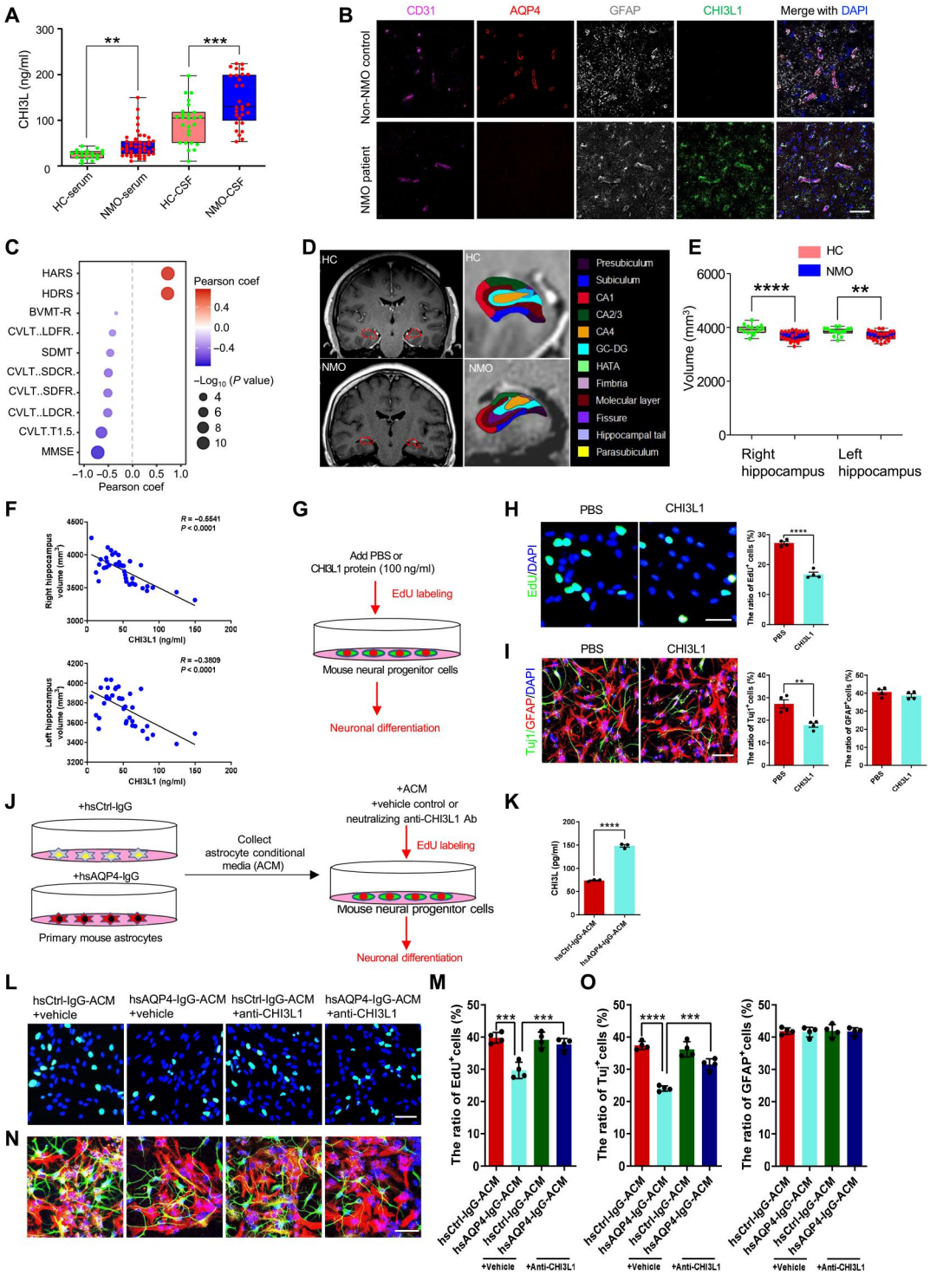

Fig. 2. The effects of astrocyte-secreted CHI3L1 on hippocampal function and neurogenesis. (**A**) Measurements of serum and CSF CHI3L1 levels in healthy controls (HCs) and NMO patients. HC-serum, $n = 20$; NMO-serum, $n = 44$; HC-CSF, $n = 26$; NMO-CSF, $n = 29$. (**B**) Representative images of biopsied human brain tissues from a non-NMO and an NMO patient. Scale bar, 50 μm. (**C**) Correlation between serum CHI3L1 levels and neuropsychological assessments in NMO. (**D**) Hippocampus segmentation on representative MRI head images. (**E**) Assessments of the hippocampus volume. HC, $n = 15$; NMO, $n = 23$. (**F**) Correlation between hippocampus volume and serum CHI3L1 levels in NMO. $n = 38$. (**G**) Schematic diagram for analyses of proliferation and neuronal differentiation of NSCs, with or without CHI3L1 treatment. (**H**) Representative images and quantification of NSC proliferation (EdU), with or without CHI3L1 treatment. Scale bars, 100 μm. $n = 4$. (**I**) Representative images and quantification of NSC differentiation by the neuronal (Tuj1) and glial (GFAP) markers, with or without CHI3L1 treatment. Scale bars, 100 μm. $n = 4$. (**J**) Schematic diagram for analyses of NSC proliferation and neuronal differentiation, with or without astrocyte-secreted CHI3L1. (**K**) ELISA measurements of secreted CHI3L1 levels in the ACM harvested from hsCtrl-IgG– or hsAQP4-IgG–treated astrocytes. (**L**) Representative images of proliferating NSCs (EdU^+) grown in hsCtrl-IgG– or hsAQP4-IgG–treated ACM, without or with the clearance of CHI3L1 (by anti-CHI3L1 neutralizing antibodies). Scale bars, 100 μm. (**M**) Quantification of NSC proliferation. $n = 4$. (**N**) Representative images of newly differentiated neurons from ACM-treated NSCs, without or with CHI3L1 clearance. Scale bars, 100 μm. (**O**) Quantification of neuronal differentiation of NSCs. $n = 4$. Bar graphs presented in means ± SEM; (A), (E), (H), (I), and (K), by Student's t test; [(M) to (O)], by one-way ANOVA and Tukey's post hoc analyses; (C), by Pearson correlation coefficient. $^{**}P < 0.01$, $^{***}P < 0.001$, $^{****}P < 0.0001$.

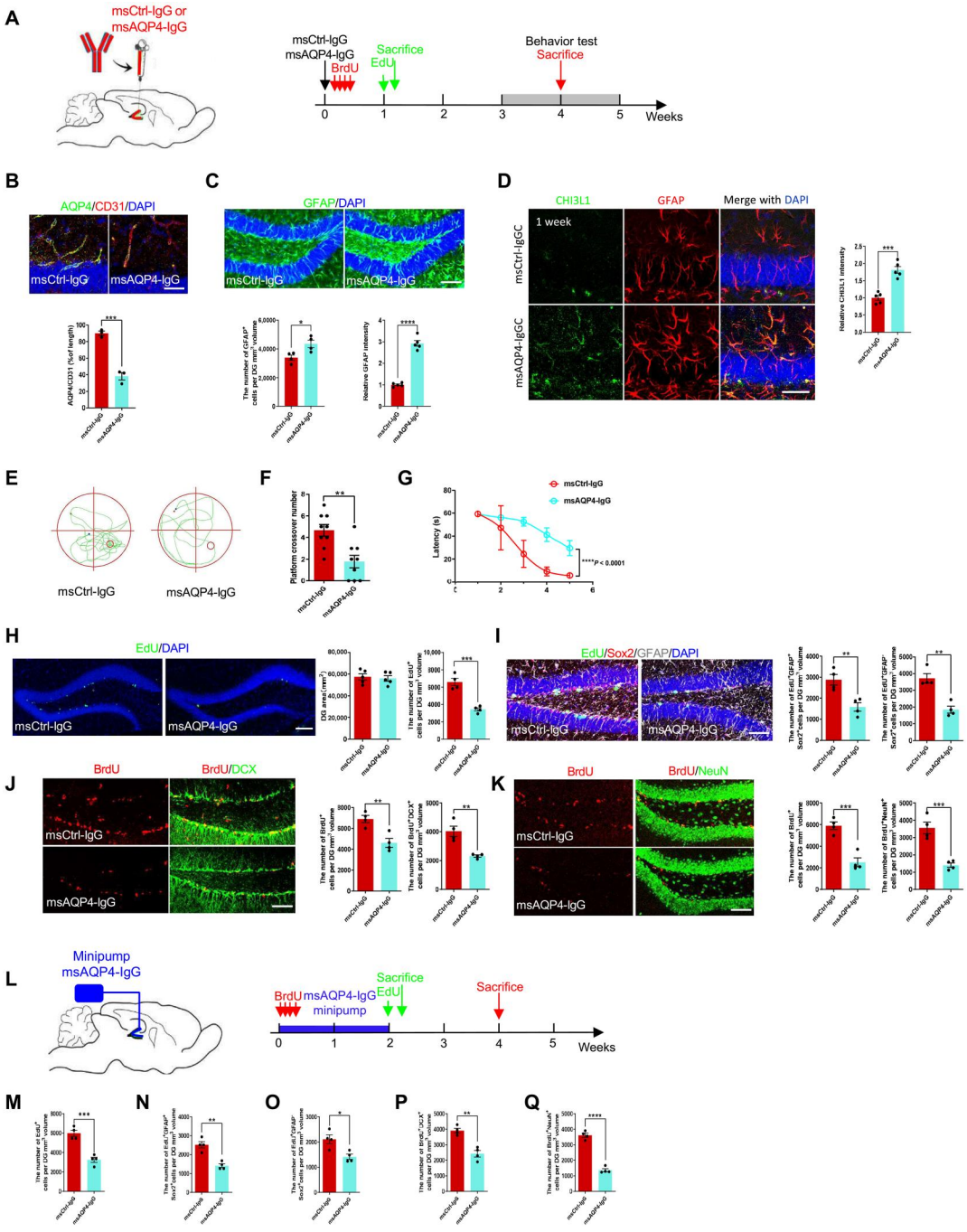

Fig. 3. The effects of immune-mediated astroglial activation on hippocampal neurogenesis and cognitive performance. (**A**) Schematic diagram of assays for hippocampal neurogenesis (EdU and BrdU labeling) and cognitive performance with stereotaxic injections of control (msCtrl-IgG) or monoclonal mouse anti-AQP4 antibodies (msAQP4-IgG). (**B**) Analysis of AQP4 expression in astrocytes [at end-feet along microvessels ($CD31^+$)] in msCtrl-IgG– or msAQP4-IgG–injected hippocampus. $n = 3$ animals. Scale bar, 20 μm. (**C**) Quantification of astrogliosis (GFAP) by msAQP4-IgG treatment within the volume of injected DG determined by 3D rendering of confocal images. $n = 3$. Scale bar, 100 μm. (**D**) Assessment of CHI3L1 expression in astrocytes induced by msAQP4-IgG. $n = 3$. Scale bar, 20 μm. (**E**) Representative movement paths of msCtrl-IgG– or msAQP4-IgG–injected mice in MWM. (**F**) MWM platform crossing numbers. $n = 9$. (**G**) Escape latencies to find the platform in MWM. $n = 9$. (**H**) Representative images and analyses of the proliferating cells (EdU^+) in hippocampus SGZ. $n = 5$. Scale bar, 100 μm. (**I**) Quantification of radial glia–like NSCs ($EdU^+GFAP^+Sox2^+$) and transiently amplifying progenitor-like cells ($EdU^+GFAP^-Sox2^+$). $n = 4$. Scale bar, 100 μm. (**J**) Analysis of immature neurons (DCX^+) differentiated from NSCs ($BrdU^+$) after msCtrl-IgG or msAQP4-IgG injections. $n = 4$. Scale bar, 100 μm. (**K**) Analysis of mature neurons ($NeuN^+$) differentiated from NSCs ($BrdU^+$) after msCtrl-IgG or msAQP4-IgG injections. $n = 4$. Scale bar, 100 μm. (**L**) Schematic diagram of assays for hippocampal neurogenesis and cognitive performance with mini-pump infusion of msCtrl-IgG or msAQP4-IgG. (**M** to **O**) Quantification of total proliferating (EdU^+) cells, radial glia–like NSCs ($EdU^+GFAP^+Sox2^+$), and transiently amplifying progenitor-like cells ($EdU^+GFAP^-Sox2^+$) in IgG-infused DG. $n = 4$. (**P** and **Q**) Quantification of newborn immature ($BrdU^+DCX^+$) neurons and mature ($BrdU^+NeuN^+$) neurons in IgG-infused DG. $n = 4$. Bar graphs presented in means ± SEM; (B) to (D), (F), (H) to (K), and (M) to (Q), by Student's t test; (G), by two-way ANOVA with Tukey's multiple comparisons. $^*P < 0.05$, $^{**}P < 0.01$, $^{***}P < 0.001$.

5-ethynyl-2′-deoxyuridine (EdU) by intraperitoneal injections and were sacrificed at two different time points: 1 week for the EdU groups (2 hours after the labeling) and 4 to 5 weeks for the BrdU groups after behavioral tests (Fig. 3A, green and red arrows, respectively). One week after the stereotaxic IgG delivery, we first found that msAQP4-IgG injection successfully led to the loss of AQP4 expression in the vicinity of the injection site (fig. S3A). We also observed that, while brain vasculature remained unperturbed (labeled by the endothelial marker CD31), the msAQP4-IgG group exhibited the NMO diagnostic feature of reduced coverage of $AQP4^+$ astrocyte end-feet (along the microvessels), as compared to controls of msCtrl-IgG group (Fig. 3B). Consistent with our findings on primary astrocytes (Fig. 1D) and biopsied human brain tissues (Fig. 2B), the msAQP4-IgG instigated a marked induction

of GFAP (Fig. 3C) and CHI3L1 (Fig. 3D) in astrocytes. Such msAQP4-IgG effect was long-lasting and detected 5 weeks after the stereotaxic injection (fig. S3B). We also dissected out the injected hippocampal tissues without fixation and lysed them for further analyses. The CHI3L1 level was noticeably higher in the lysates from the msAQP4-IgG group after the enzyme-linked immunosorbent assay (ELISA) measurements (fig. S3C). We further confirmed the proinflammatory features we characterized in vitro (fig. S3D) with qPCR assays, showing an induction in almost all tested neuroinflammation and astrocyte activation genes identified from our transcriptomic meta-analyses (Fig. 1, H to J).

We continued to characterize the cognitive effects from immune-mediated astrocyte activation by performing behavioral assays that correspond to the cognitive impairment and hippocampal dysfunction observed in NMO patients (Fig. 2C and fig. S2C). Four to 5 weeks after the stereotaxic transfer of IgGs (Fig. 3A, red arrows), the injected mice underwent standardized behavioral assays of the open field test (OFT) and the Morris water maze (MWM), as described previously (*35*). Compared with the control msCtrl-IgG group (fig. S3E), the msAQP4-IgG group of mice overall traveled shorter total distances (fig. S3F) and spent less time in the center area (fig. S3G) in the OFT. Such defects indicated a decrease in locomotor activity and an increase in anxiety-like behavior owing to the brain inflammation. The MWM task, a widely used assay to assess the hippocampus-dependent spatial learning and memory (Fig. 3E), revealed in the msAQP4-IgG group the faulty behaviors with decreased numbers of the platform crossing (Fig. 3F) and extended escape latencies (Fig. 3G). These behavioral findings, together with the histopathological data above (Fig. 3, B to D), demonstrated that our AQP4 antibody–induced astrocytopathy mouse model recapitulated key aspects of NMO disease manifestations (Fig. 2, A to D).

To investigate whether the cognitive dysfunction stemming from immune-mediated neuroinflammation would be associated with a change in neurogenesis, we checked the proliferation and neuronal differentiation of NSCs within the SGZ by standardized methodology for quantification of neurogenesis (*55*). One week after the injections of antibodies, the EdU-labeled mice from msCtrl-IgG and msAQP4-IgG groups had comparable sizes of dentate gyrus (DG) after the acute experiment period (Fig. 3A, green arrows), but the msAQP4-IgG group showed much fewer EdU^+ cells (Fig. 3H). Further analyses showed that the populations of the radial glia–like NSC cells (triple-labeled by $EdU^+GFAP^+Sox2^+$) and the transiently amplifying progenitor cells ($EdU^+GFAP^-Sox2^+$) were both reduced (Fig. 3I), suggesting an inhibition of NSC proliferation. Moreover, to determine the effect on neuronal differentiation of NSC after our single-dose AQP4-IgG administration, we analyzed the BrdU-labeled mice, labeling 4 to 5 weeks after the intrahippocampal delivery of msCtrl-IgG or msAQP4-IgG (Fig. 3A, red arrows). The numbers of newly differentiated immature neurons ($BrdU^+DCX^+$) and mature neurons ($BrdU^+NeuN^+$) were appreciably lower (Fig. 3, J and K). Consistent with our in vitro results (Fig. 2, G to O), our findings here demonstrated a defective process of neurogenesis in the neuroinflammation triggered by the immune response.

In parallel to the mouse model based on stereotaxic injections of antibodies, we also leveraged our established technique of mini-osmotic pump implantation (*34*, *56*) to develop the other passive transfer mouse model. msCtrl-IgG or msAQP4-IgG was chronically infused into the hippocampal regions of young adult wild-type mice on both sides at the age of 8 weeks (Fig. 3L). The BrdU labeling was administered soon after the start of IgG perfusion for us to evaluate the neuronal differentiation of NSCs (Fig. 3L, red arrows); EdU was given at the end of the 2-week perfusion and followed by sacrifice and fixation of the brain to examine NSC proliferation (Fig. 3L, green arrows). In the EdU-labeled hippocampal slices, the perfusion of msAQP4-IgG, as compared to the msCtrl-IgG control condition, resulted in a decline in the numbers of total proliferating cells (fig. S3H and Fig. 3M), radial glia–like cells (Fig. 3N,) and transiently amplifying progenitor cells (Fig. 3O) in the SGZ. Furthermore, at the end of the fourth week of experimentation, our quantification of BrdU labeling and neuronal marker expression showed that the msAQP4-IgG perfusion contracted the cell populations of newly differentiated immature neurons (fig. S3I and Fig. 3P) and mature neurons (fig. S3J and Fig. 3Q). Together, two different approaches —stereotaxic injection and chronic perfusion—of msAQP4-IgG delivery generated results that mirrored each other and jointly suggested the inhibition of adult hippocampal neurogenesis in immune-mediated astrocyte activation, potentially mediated by the secreted CHI3L1 in a paracrine manner.

CHI3L1 is sufficient to reduce neurogenesis and impair hippocampal-dependent learning behaviors in young adult mice

We showed that, among the plethora of proinflammatory secretory proteins released by activated astrocytes (Fig. 1H), CHI3L1 is important for the inhibition of NSC proliferation and differentiation following inflammatory responses in vitro (Fig. 2, G to I and J to O, and fig. S2, F and G). To directly test our hypothesis that CHI3L1 is the major player for the hippocampal dysfunction and impaired neurogenesis caused by neuroinflammation in vivo, we overexpressed CHI3L1 in the mouse hippocampus and assayed the cognitive performance and NSC proliferation and differentiation. We constructed lentiviral vectors expressing CHI3L1 plus enhanced green fluorescent protein (eGFP) (Lenti-CHI3L1, eGFP-2A-CHI3L1 with cytomegalovirus promoter) or eGFP alone as a control (Lenti-Ctrl), and stereotaxically injected the prepared lentiviruses into the DG of 8-week-old wild-type mice (Fig. 4A). Following the lentiviral injections, the labeling of BrdU or EdU was carried out at the specific time points to allow our measurements of NSC proliferation and neuronal differentiation (Fig. 4B). Two weeks after the injections, we sacrificed a subset of mice, dissected out the injected hippocampal tissues without fixation, and confirmed the overexpression of CHI3L1 by immunoblotting on the hippocampal lysates (Fig. 4C). We then probed the effect of CHI3L1 overexpression on cognitive function and performed the behavioral assays 4 to 6 weeks after the lentiviral injections (Fig. 4B, red arrows). In the OFT (fig. S4A), mice overexpressing CHI3L1 traveled for a total distance significantly shorter than what controls (expressing eGFP alone) did, indicating a reduced level of locomotor activity (fig. S4B). Tracing the movements of crossing the central area showed that CHI3L1 overexpression led to a strong preference for the edge and corner locations, which suggested an elevated level of anxiety-like behavior (fig. S4C). Meanwhile, MWM (Fig. 4D) revealed that CHI3L1-overexpressing mice made less platform crossovers (Fig. 4E) and took significantly more time to escape (Fig. 4F), as compared to the control group. These behavioral changes induced by CHI3L1 highly resemble our findings on the

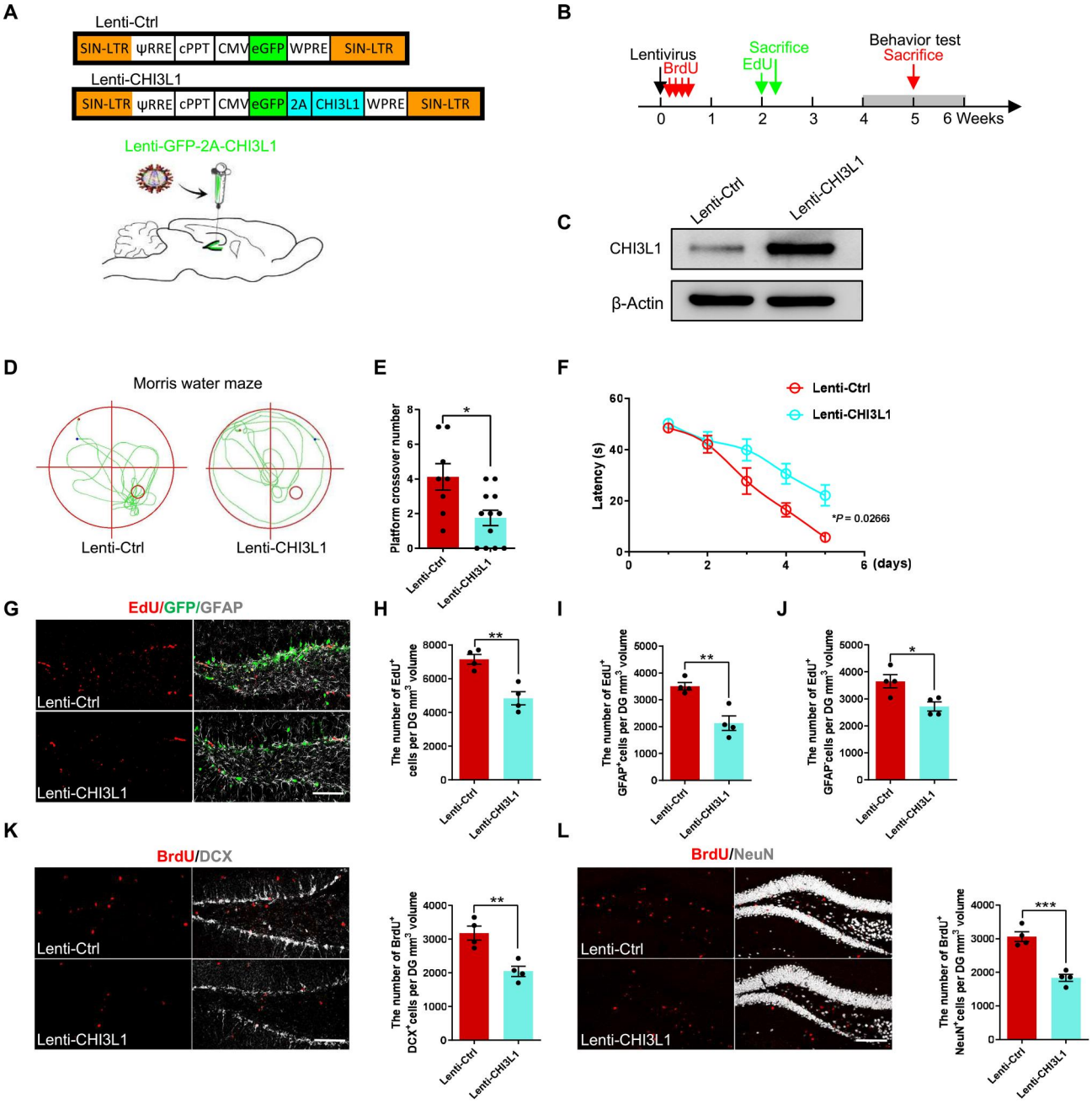

Fig. 4. The effects of CHI3L1 overexpression on hippocampal neurogenesis and cognitive performance. (**A**) Lentiviral vectors of control (Lenti-Ctrl) or CHI3L1expression (Lenti-CHI3L1), with eGFP coexpression. (**B**) Timeline of assays for NSC proliferation (by EdU labeling, green arrows) and neuronal differentiation (by BrdU labeling) and their behavioral consequences (red arrows) in control or CHI3L1-overexpressing mice. (**C**) CHI3L1 expression by immunoblotting of hippocampal lysates from control or CHI3L1-overexpressing mice. (**D** and **E**) Representative movement paths and quantification of MWM crossing number control for CHI3L1-overexpressing mice. Lenti-Ctrl, $n = 8$ animals. Lenti-CHI3L1, $n = 12$. (**F**) Escape latencies to find the platform in MWM. Lenti-Ctrl, $n = 8$. Lenti-CHI3L1, $n = 12$. (**G**) Representative images of Lenti-Ctrl– or Lenti-CHI3L1–injected hippocampus immunostained for NSC proliferation. Scale bar, 100 μm. (**H** to **J**) Quantification of total proliferating cells (EdU^+), radial glia–like NSCs (EdU^+GFAP^+), and transiently amplifying progenitor-like cells. $n = 4$ animals. (**K**) Representative images and quantification of newborn immature neurons ($BrdU^+$ DCX^+) in Lenti-Ctrl– or Lenti-CHI3L1–injected hippocampus. $n = 4$. Scale bar, 100 μm. (**L**) Representative images and quantification of newborn immature neurons ($BrdU^+$ $NeuN^+$) in Lenti-Ctrl– or Lenti-CHI3L1–injected hippocampus. $n = 4$. Scale bar, 100 μm. All data presented in means ± SEM; bar graphs (E) and (H) to (L), by Student's *t* test for two-group comparisons; (F), by two-way ANOVA with Tukey's multiple comparisons test. Nonsignificant comparisons are not identified. $^*P < 0.05$, $^{**}P < 0.01$, $^{***}P < 0.001$.

msAQP4-IgG–treated mice (Fig. 3, E to G, and fig. S3, E to G). We next sought to investigate the effect of CHI3L1 overexpression on neurogenesis and analyzed the fixed and immunostained hippocampal slices by confocal imaging. In the EdU-labeled mice (Fig. 4B, green arrows), we detected abundant eGFP expression in the dentate gyri from both control (eGFP alone) and CHI3L1 overexpression (CHI3L1 plus eGFP) groups and validated the successful lentiviral transduction 2 weeks after the lentiviral injections (Fig. 4G). To assess the proliferation, we quantified the EdU signals and noted a decrease in the number of EdU^+ cells in the SGZ (Fig. 4, G and H). We classified these proliferating cells by costaining of GFAP and by the typical NSC morphology, and we found that CHI3L1 overexpression lessened the radial glia–like cells (Fig. 4I) as well as the transiently amplifying progenitor-like cells (Fig. 4J) in the examined hippocampal tissues. We again used the fluorescence signals from BrdU and markers for immature and mature neurons to evaluate the neuronal differentiation from NSCs (Fig. 4B, red arrows). Overexpression of CHI3L1 reduced both the pools of newly differentiated immature neurons (Fig. 4K) and mature neurons (Fig. 4L), yielding one more line of evidence for the inhibitory role of CHI3L1 for adult hippocampal neurogenesis. The virtual reproduction of the msAQP4-IgG effects (Fig. 3) by CHI3L1 overexpression here (Fig. 4) corroborates the notion that CHI3L1 is sufficient to convey the detrimental effects of neuroinflammation on hippocampal function and cognitive performance.

CHI3L1 cooperated with CRTH2 receptor to inhibit adult hippocampal neurogenesis by reducing β-catenin signaling

To delineate the CHI3L1 signaling mechanism for the impaired neurogenesis in neuroinflammation, we pursued identifying the responsible receptor and downstream pathway in NSCs. Uncovered by our collaborative group and others, CHI3L1 functions through a set of defined transmembrane receptors, such as IL-13 receptor α2 (IL-13Rα2), transmembrane protein 219 (TMEM219) (*7*), and chemoattractant receptor homologous with T helper 2 (T_H2) cell (CRTH2) (*57*), by activating several signaling cascades (Fig. 5A). To uncover potential CHI3L1 receptors on NSCs, we first performed immunostaining to analyze the expression patterns of the individual candidate receptors in the DG in wild-type young adult mouse brains. Unexpectedly, the best characterized CHI3L1 receptor IL-13Rα2 (*12*, *51*) was minimally expressed in NSCs (fig. S5A), and the TMEM219 expression was similarly low (fig. S5B). CRTH2 instead was abundantly expressed in NSCs and to a lesser extent in the immature neurons but not in mature neurons (Fig. 5B). For better visualization, we turned to the cultured NSCs and confirmed the expression of CRTH2 (Fig. 5C). After the recognition of CRTH2 as a potential CHI3L1 receptor on NSCs, we focused on the specific downstream pathway that is mediated by glycogen synthase kinase-3β (GSK-3β) and β-catenin (Fig. 5A). β-Catenin is a critical transcription factor in Wnt signaling and governs the process of adult hippocampal neurogenesis (*58*). GSK-3β, a serine/threonine protein kinase stimulated by CRTH2 activation (*59*), phosphorylates and targets β-catenin for proteasomal degradation unless the kinase function is inactivated by phosphorylation at Ser^9 (*60*). We analyzed the perturbation of GSK-3β and β-catenin expression in purified mouse NSCs treated with recombinant CHI3L1. CHI3L1 treatment rapidly accumulated active GSK-3β with a concomitant reduction in the inhibitory Ser^9 phosphorylation within 30 min (Fig. 5D). CHI3L1 simultaneously caused a prolonged decrease in the β-catenin protein level that persisted more than 2 hours (Fig. 5D), indicating destabilization and degradation triggered by the increased GSK-3β kinase activity, which would be directly downstream to CRTH2 activation by CHI3L1 binding.

To confirm the participation of CRTH2 receptor in the identified CHI3L1 signaling pathway, we designed short hairpin RNAs (shRNAs) targeting all three tested receptors, CRTH2, IL-13Rα2, and TMEM219, and lentivirally transduced them (shCRTH2, shIL-13Rα2, and shTMEM219) and a scrambled nontargeting control shRNA (shCtrl) individually in cultured mouse NSCs (Fig. 5E, with coexpression of eGFP to ensure adequate transduction efficiency, >99%). The knockdown efficiency was satisfactory at a level of 75 to 90% across all designed shRNAs (Fig. 5F and fig. S5, C and D). Upon CHI3L1 treatment for 2 hours, the shRNA-mediated knockdown of CRTH2 in NSCs maintained the Ser^9 inhibitory phosphorylation of GSK-3β and stabilized β-catenin from degradation (Fig. 5G), suggesting that CRTH2 depletion blocked the CHI3L1 effects on GSK-3β activation and β-catenin inhibition. We continued to investigate whether the CRTH2-dependent signaling pathway would be necessary for the CHI3L1-induced inhibition of NSC proliferation and neuronal differentiation. In NSC cultures expressing control shRNA, CHI3L1 treatment reduced the numbers of proliferating cells (Fig. 5H) as well as the newborn neurons (Fig. 5I). The cultured NSCs made deficient of CRTH2 by shRNA, however, displayed unchanged levels of proliferation (Fig. 5H) and neuronal differentiation (Fig. 5I). Conversely, the knockdown of the receptors IL-13Rα2 and TMEM219 did not render NSCs insensitive to CHI3L1 treatment and still showed the suppressed proliferation (fig. S5E) and neuronal differentiation (fig. S5F). Together, we demonstrated that CHI3L1 engages CRTH2 receptor and activates GSK-3β, which in turn destabilizes β-catenin and thus perturbs the transcriptional network for neurogenesis driven by β-catenin (Fig. 5J).

To substantiate the involvement of GSK-3β in the CHI3L1 signaling pathway, we used a selective, potent inhibitor of GSK-3β, TWS119 (*61*), and study its effect on hippocampal neurogenesis in neuroinflammation. We administered TWS119 intraperitoneally in wild-type young adult mice immediately after the stereotaxic injections of msCtrl-IgG or msAQP4-IgG and used EdU and BrdU labeling to measure the NSC proliferation and neuronal differentiation (Fig. 5K). We noticed that TWS119 treatment, as compared to vehicle control, increased the numbers of proliferating cells (Fig. 5L, EdU^+) including the radial glia–like NSC cells (fig. S5G and Fig. 5M) and the transiently amplifying progenitor cells (fig. S5G and Fig. 5N). TWS119 also enhanced neuronal differentiation of NSCs inhibited by msAQP4-IgG, according to our quantifications of BrdU-labeled NSCs, giving rise to immature and mature neurons (fig. S5, H and I, and Fig. 5, O to Q). Collectively, our findings depicted an original CHI3L1 signaling mechanism and also suggested that blocking the CHI3L1 receptor or downstream signaling mediators would reinstate neurogenesis under the circumstance of astrocyte activation in neuroinflammation.

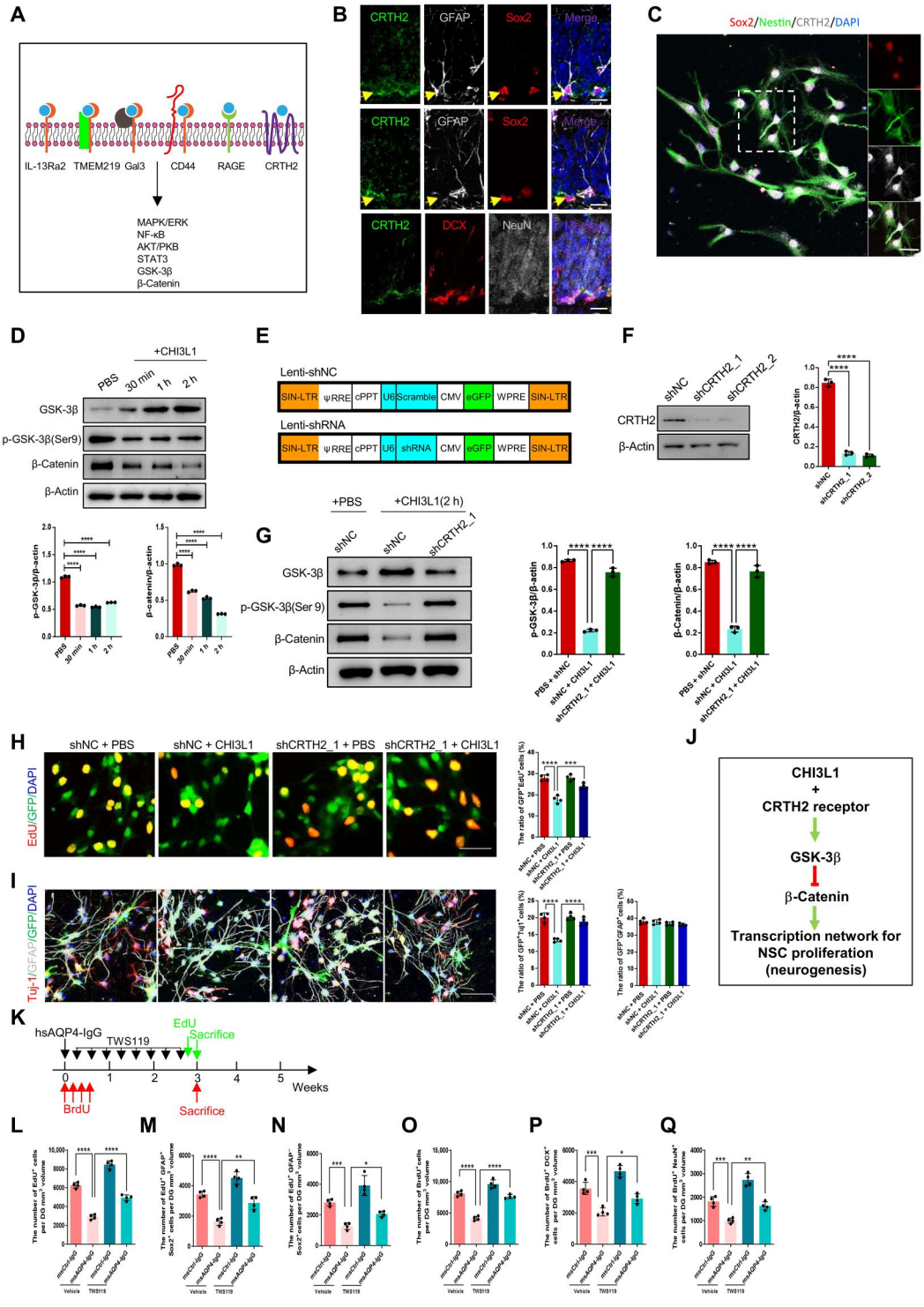

Fig. 5. The CHI3L1 receptor and downstream pathway in NSCs to regulate neurogenesis in neuroinflammation. (**A**) Summary of CHI3L1 receptors and downstream signaling pathways. (**B**) Expression of CRTH2 receptor in NSCs (GFAP$^+$Sox2$^+$) but not immature (DCX$^+$) or mature (NeuN$^+$) neurons in adult hippocampus. Scale bars, 20 μm. (**C**) CRTH2 expression in cultured NSCs (Sox2$^+$Nestin$^+$). (**D**) Activation of GSK-3β (reduced inhibitory serine-9 phosphorylation) and inhibition of β-catenin (increased degradation) in NSC cultures treated with CHI3L1 (100 ng/ml). $n = 3$. (**E**) Lentiviral vectors to express two shRNAs for CRTH2 knockdown (Lenti-shCRTH2, shCRTH2_1, and shCRTH2_2) and a control shRNA (Lenti-shNC). (**F**) shRNA-mediated CRTH2 knockdown efficiency. $n = 3$. (**G**) CRTH2 knockdown effect on GSK-3β/β-catenin pathway activation by CHI3L1 (2-hour treatment). $n = 3$. (**H**) CRTH2 knockdown effect on NSC proliferation in shRNA-expressing cultures, with or without CHI3L1 for 3 days. $n = 4$. Scale bars, 100 μm. (**I**) CRTH2 knockdown effect on NSC differentiation into neurons (Tuj1$^+$) and glia (GFAP$^+$) in shRNA-expressing cultures, with or without CHI3L1 for 3 days. $n = 4$. Scale bars, 100 μm. (**J**) Identified CHI3L1 signaling pathway inhibitory to neurogenesis: CHI3L1 binds to CRTH2 receptor and activates GSK-3β that in turn phosphorylates and destabilizes β-catenin and leads to reduced transcriptional activities for neurogenesis. (**K**) Timeline for assays of NSC proliferation and neuronal differentiation in msCtrl-IgG– or msAQP4-IgG–injected mice, receiving a potent GSK-3β inhibitor, TWS119 (30 mg/kg), intraperitoneally daily for 3 weeks. (**L** to **N**) Quantification of total proliferating cells (EdU$^+$), radial glia–like NSCs (EdU$^+$GFAP$^+$), and transiently amplifying progenitor-like (EdU$^+$GFAP$^-$) cells. $n = 4$. (**O** to **Q**) Quantification of proliferating cells (BrdU$^+$) at the time of hsAQP4-IgG injection, newborn immature neurons (BrdU$^+$DCX$^+$), and mature neurons (BrdU$^+$NeuN$^+$). $n = 4$. All bar graphs presented in means ± SEM and analyzed by one-way ANOVA and Tukey's post hoc analyses. *$P < 0.05$, **$P < 0.01$, ***$P < 0.001$, ****$P < 0.0001$.

Depletion of CHI3L1 secreted by astrocytes improves adult hippocampal neurogenesis and function in immune-mediated neuroinflammation

We continued to test whether this CHI3L1–CRTH2–GSK-3β/β-catenin signaling cascade could be modulated to modify the inhibitory effect of CHI3L1 on hippocampal function and neurogenesis in vivo. As CHI3L1 is primarily secreted by activated astrocytes, we first targeted the astroglial expression of CHI3L1 in the immune-mediated neuroinflammation. We used our validated *Chi3l1*-floxed (*Chil1*$^{f/f}$) mouse strain (*11*, *62*) and achieved astrocyte-specific conditional knockout by adeno-associated virus (AAV) injections transducing Cre recombinase under the control of GFAP promoter (Fig. 6A, with coexpression of eGFP for our evaluation of lentiviral transduction efficiency). Specifically, these AAVs were stereotaxically injected into the hippocampal regions of the homozygous mutant mice (*Chil1*$^{f/f}$, exon 5 flanked by l*oxP* sites) or heterozygous littermates (*Chil1*$^{f/+}$) at the age of 8 weeks (Fig. 6A). We first checked the specificity and efficiency of the intended conditional knockout in astrocytes. Two weeks after the AAV injections (Fig. 6A, first sacrifice), we made the observation that most GFP$^+$ cells were colabeled with GFAP signals, indicating that nearly all AAV-transduced cells were astrocytes (Fig. 6B). The brains of a subset of the AAV-injected *Chil1*$^{f/+}$ and *Chil1*$^{f/f}$ mice were harvested without fixation, and then their hippocampi were dissected and lysed to measure the mRNA and protein levels of CHI3L1. The knockout efficiency was more than 80% in comparing the *Chil1*$^{f/f}$ samples to the *Chil1*$^{f/+}$ ones (Fig. 6C and fig. S6A). Having validated the astrocyte-specific depletion of CHI3L1 in the hippocampus, we carried out the experiments to assess the hippocampal function by using the model of stereotaxic IgG injection, as we described above (Fig. 3, A to K). We stereotaxically delivered msCtrl-IgG or msAQP4-IgG into the hippocampal region after a 4-week recovery from the AAV-mediated CHI3L1 depletion and performed the behavioral tests at week 8 (Fig. 6A). In the CHI3L1-expressing *Chil1*$^{f/+}$ mice, we noticed that msAQP4-IgG provoked the abnormalities of lower locomotor activity, anxiety-like behaviors, and impaired memory operation, as in the wild-type mice receiving intrahippocampal injection of msAQP4-IgG (fig. S3, E to G, and Fig. 3, E to G): OFT (fig. S6B) showed a shorter total travel distance (fig. S6C) and the reluctance to explore and cross the central area (fig. S6D), while MWM (Fig. 6D) revealed a decreased number of the platform crossing (Fig. 6E) and extended escape latencies (Fig. 6F). In the *Chil1*$^{f/f}$ mice undergoing the diminution of CHI3L1 by AAV-Cre, the aforementioned behavioral abnormalities induced by msAQP4-IgG were much alleviated, according to our analyses of OFT (fig. S6, B to D) and MWM (Fig. 6, D to F). These results of CHI3L1 deletion, in conjunction with our findings on CHI3L1 overexpression (Fig. 4, A to F), firmly argued for the inhibitory role of astrocyte-secreted CHI3L1 on the hippocampal function in an inflammatory condition with astroglial activation.

We next sought to decipher the effect of astrocyte-secreted CHI3L1 on hippocampal neurogenesis in immune-mediated neuroinflammation by labeling the *Chil1*$^{f/+}$ and *Chil1*$^{f/f}$ mice with BrdU and EdU after the astroglial activation by mini-pump perfusion of msAQP4-IgG (Fig. 6G). BrdU was administrated right after the AAV injections in one group of *Chil1*$^{f/+}$ and *Chil1*$^{f/f}$ mice, and EdU was given 4 weeks later in the other group to facilitate our measurements of NSC proliferation (by EdU labeling) and differentiation in neurons (by BrdU). msCtrl-IgG or msAQP4-IgG was chronically perfused into the DG for a period of 2 weeks by a mini-pump to elicit astrocyte activation and immune-mediated neuroinflammation. The treated mice were then sacrificed at the indicated times to prepare the hippocampal slices for our confocal microscopy (Fig. 6G). At the completion of IgG perfusion, we found that msAQP4-IgG significantly decreased the number of total proliferating cells in the SGZ from the *Chil1*$^{f/+}$ groups but did not alter that from the *Chil1*$^{f/f}$ groups (Fig. 6H). The similar msAQP4-IgG effect was observed on the number of proliferating radial glia–like NSCs (Fig. 6I). We next analyzed the BrdU-labeled NSC lineage cells for their expression of immature and mature neuronal markers and NeuN. As expected, msAQP4-IgG perfusion diminished both the newly differentiated immature and mature neurons in the CHI3L1-expressing hippocampal tissues from the *Chil1*$^{f/+}$ groups (Fig. 6, J and K). Of note, the CHI3L1 depletion in astrocytes counteracted the inhibitory effect from msAQP4-IgG and made no obvious alternation in the pools of immature and mature neurons as compared to the control msCtrl-IgG group (Fig. 6, J and K).

Moreover, we used the anti-CHI3L1 antibodies (Fig. 2, L to O) to neutralize the secreted CHI3L1 to substantiate the neuroprotective effect from blocking the CHI3L1 signaling function. We coinjected msCtrl-IgG or msAQP4-IgG plus vehicle control PBS or anti-CHI3L1 IgG into the hippocampi of wild-type young adult mice and evaluated the situation of neurogenesis (Fig. 6L). We noted that the neutralization of CHI3L1 relieved the msAQP4-induced suppression on NSC proliferation (fig. S6E and Fig. 6, M to O) and neuronal differentiation (fig. S6, F and G, and Fig. 6, P and Q). These data firmly supported our hypothesis that the astrocyte-secreted CHI3L1 negatively affects hippocampal neurogenesis and function in immune-mediated neuroinflammation and that the deletion of CHI3L1 in astrocytes could reverse such inflammatory sequelae.

Inhibition of CHI3L1 receptor pathway rescues the neurogenic and cognitive deficits in immune-mediated neuroinflammation

We further investigated whether blocking the CHI3L1 signaling pathway would be able to rescue the impaired neurogenesis resulting from astroglial activation in neuroinflammation. To disrupt activation of CRTH2 receptor by CHI3L1 binding, we injected the lentiviruses expressing the control shRNA or the validated shRNA against CRTH2 (Fig. 5, E to I) into the DG of the hippocampus to knock CRTH2 down in 8-week-old wild-type young adult mice (Fig. 7A). We then implanted the mini-pump for a 2-week perfusion of msCtrl-IgG or msAQP4-IgG and administered EdU and BrdU to evaluate NSC proliferation and neuronal differentiation. As expected, msAQP4-IgG induced astrocyte activation and CHI3L1 expression with or without CRTH2 knockdown (fig. S7, A and B). In the control groups (shCtrl), msAQP4-IgG markedly attenuated NSC proliferation, as the numbers of total proliferating cells and proliferating radial glia–like cells were both lowered (Fig. 7B). In contrast, CRTH2 knockdown abolished such repressive influence from msAQP4-IgG and led to little or no apparent change in NSC proliferation (Fig. 7B). In neuronal differentiation assays, CRTH2 knockdown also preserved the numbers of immature and mature newborn neurons, which were both reduced in the presence of CRTH2 to convey CHI3L1 signaling in neuroinflammation (Fig. 7, C and D). Together, these findings corroborated the role of CRTH2 as a receptor for CHI3L1 signaling in NSCs and

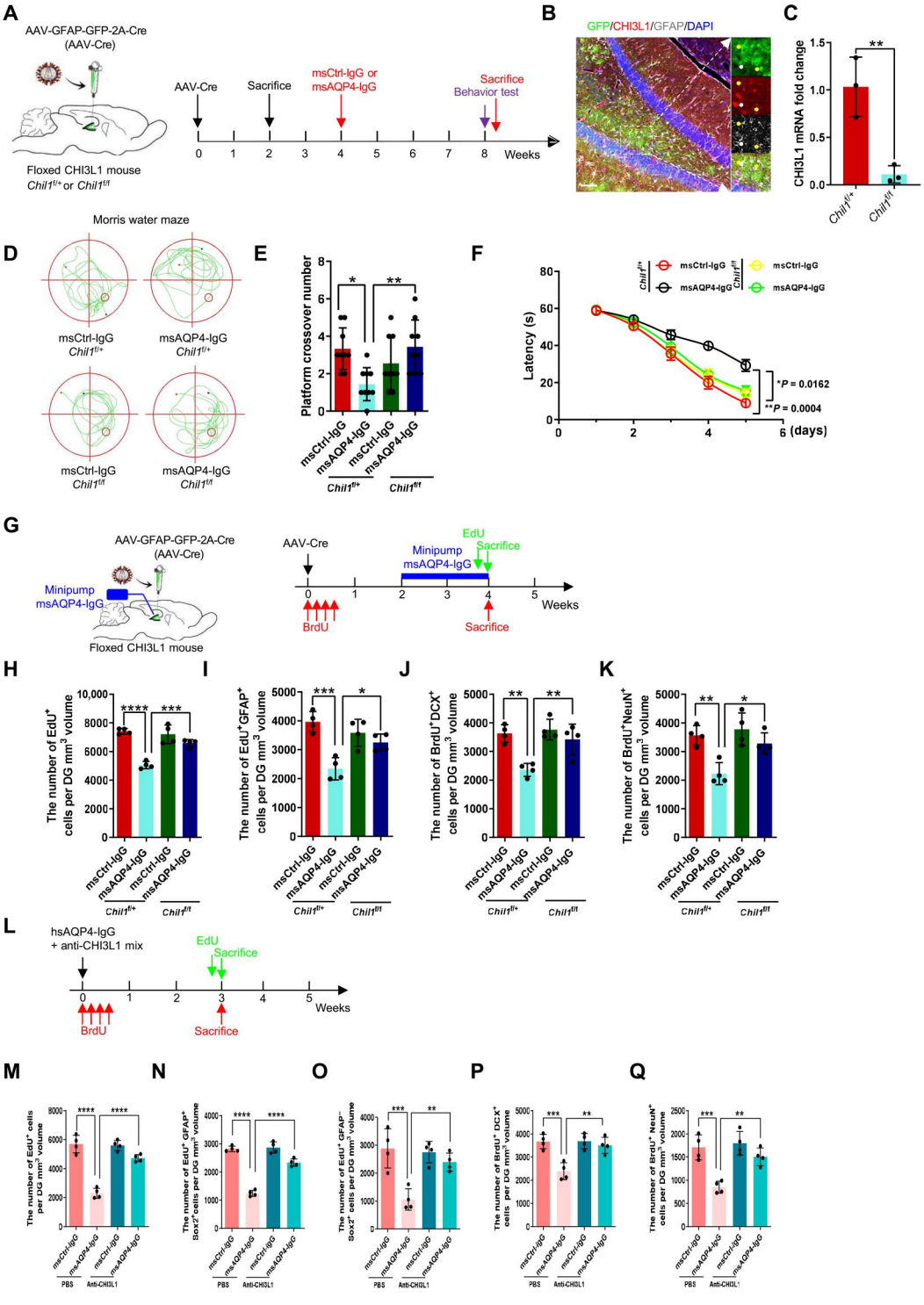

Fig. 6. The effects of astrocyte-specific CHI3L1 knockout on hippocampal neurogenesis and cognitive performance. (**A**) Schematic diagram of the astrocyte-specific CHI3L1 knockout by intra-hippocampus injections of AAVs expressing Cre recombinase plus eGFP by GFAP promoter in heterozygous (*Chil1*$^{f/+}$) or homozygous (*Chil1*$^{f/f}$) CHI3L1-floxed mice. The injected mice were sacrificed 2 weeks later for knockout efficiency or received the intra-hippocampal injections of msCtrl-IgG or msAQP4-IgG 4 weeks later. (**B**) Representative images of *Chil1*$^{f/f}$ hippocampal section expressing Cre. Scale bars, 100 μm. (**C**) Evaluation of CHI3L1 knockout efficiency by qPCR on hippocampal lysates from AAV-injected *Chil1*$^{f/+}$ and *Chil1*$^{f/f}$ mice. $n = 3$ animals. (**D**) Representative MWM movement paths of CHI3L1-expressing (*Chil1*$^{f/+}$) and CHI3L1-deficient (*Chil1*$^{f/f}$) mice receiving stereotaxic injections of msCtrl-IgG or msAQP4-IgG. (**E**) Quantification of MWM crossing numbers. $n = 9$. (**F**) Quantification of MWM escape latencies to find the platform. $n = 9$. (**G**) Schematic diagram of assays for astrocyte-specific CHI3L1 knockout effect on adult hippocampal neurogenesis affected by mini-pump infusion of msCtrl-IgG or msAQP4-IgG. (**H** and **I**) Quantification of NSC proliferation plotted by total proliferating cells (EdU$^+$) and radial glia–like NSCs (EdU$^+$GFAP$^+$). $n = 4$. (**J** and **K**) Quantification of NSC proliferation into immature (BrdU$^+$DCX$^+$) and mature (BrdU$^+$NeuN$^+$) neurons. $n = 4$. (**L**) Timeline of assays for NSC proliferation and neuronal differentiation in the msCtrl-IgG– or msAQP4-IgG–treated mice, receiving the coinjections of neutralizing antibody anti-CHI3L1 or PBS. (**M** to **O**) Quantification of total proliferating cells (EdU$^+$), radial glia–like NSCs (EdU$^+$GFAP$^+$), and transiently amplifying progenitor-like cells (EdU$^+$GFAP$^-$). $n = 4$. (**P** and **Q**) Quantification of proliferating (BrdU$^+$) cells at the time of IgG injection, newborn immature neurons (BrdU$^+$DCX$^+$), and mature neurons (BrdU$^+$NeuN$^+$). $n = 4$. All quantitative data presented in means ± SEM; (C), by Student's *t* test; (F), by two-way ANOVA with Tukey's post hoc analyses; the remaining bar graphs, by one-way ANOVA with Tukey's post hoc analyses. *P < 0.05, **P < 0.01, ***P < 0.001, ****P < 0.0001.

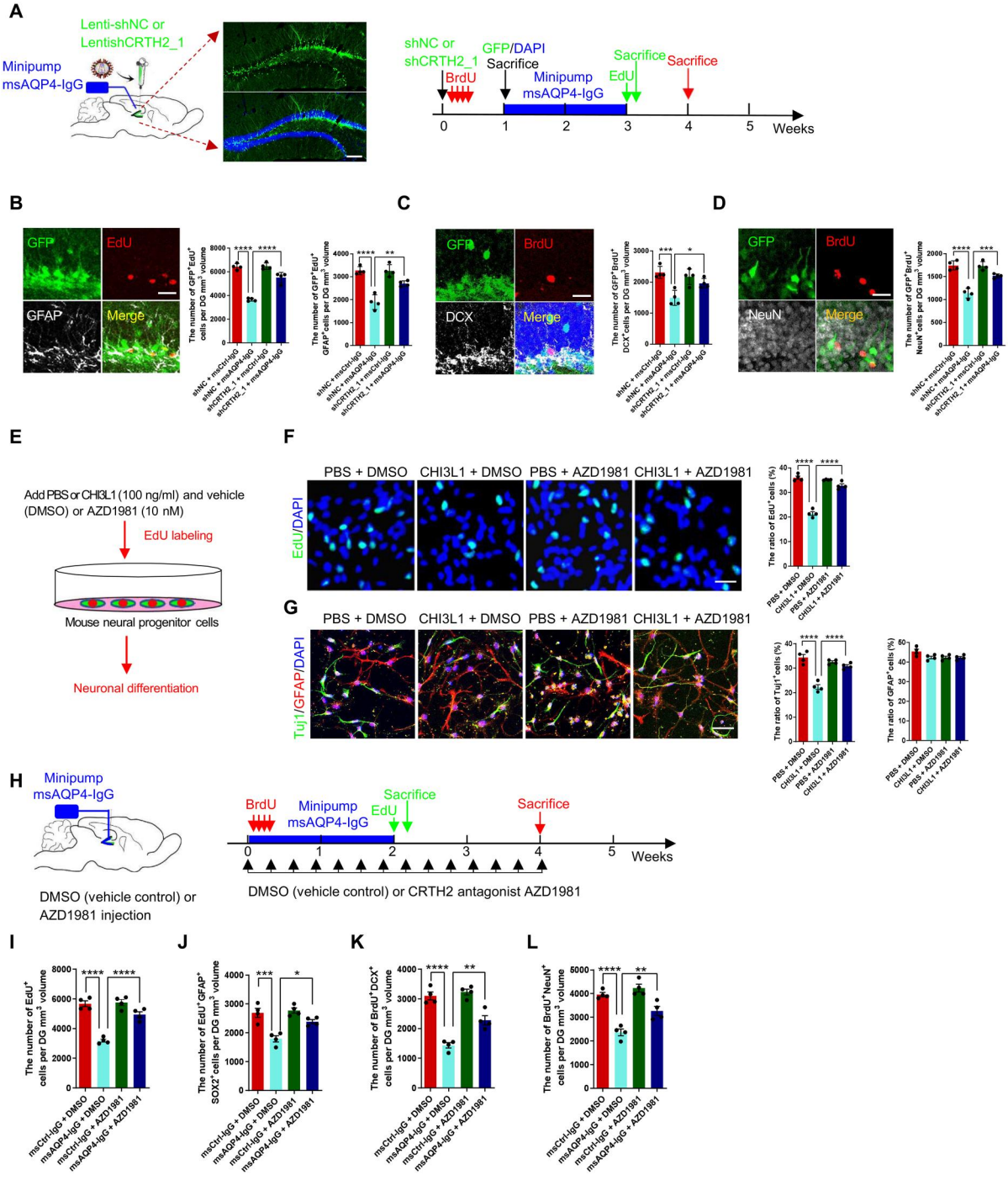

Fig. 7. The CRTH2 blockade effect on hippocampal neurogenesis and cognitive performance affected by CHI3L1. (**A**) Schematic diagram of assays for shRNA-mediated CRTH2 knockdown effect on NSC proliferation and differentiation affected by msAQP4-IgG. The lentiviruses expressing GFP together with a scrambled non-targeting control shRNA (Lenti-shNC) or an shRNA targeting CRTH2 (Lenti-shCRTH2_1). Scale bars, 100 μm. (**B**) CRTH2 knockdown effect on NSC proliferation in DG, quantified by the numbers of proliferating cells expressing an shRNA (GFP^+EdU^+) and radial glia–like NSCs (GFP^+EdU^+GFAP). $n = 4$ animals. Scale bars, 20 μm. (**C**) Quantification of shRNA-expressing (GFP^+) NSC ($BrdU^+$) differentiation into immature neurons (DCX^+) in DG. $n = 4$. Scale bars, 20 μm. (**D**) Quantification of NSC differentiation into mature neurons ($GFP^+BrdU^+NeuN^+$) in DG. $n = 4$. Scale bars, 20 μm. (**E**) Schematic diagram of in vitro assays for the effect of AZD1981, a selective CRTH2 antagonist, on neurogenesis suppressed by CHI3L1 signaling secondary to mini-pump infusion of msCtrl-IgG or msAQP4-IgG. (**F**) Quantification of NSC proliferation in DG, in the presence of CHI3L1 or PBS and with AZD1981 or DMSO. $n = 4$. Scale bars, 100 μm. (**G**) Quantification of NSC neuronal differentiation. $n = 4$. Scale bars, 100 μm. (**H**) Schematic diagram of in vivo assays for AZD1981 efficacy to rescue neurogenesis affected by msAQP4-IgG–induced CHI3L1 signaling. (**I** and **J**) Quantification of NSC proliferation by computing total proliferating cells (EdU^+) and radial glia–like NSCs ($EdU^+GFAP^+Sox2^+$) in DG. $n = 4$. (**K** and **L**) Quantification of NSC proliferation into immature ($BrdU^+DCX^+$) and mature ($BrdU^+NeuN^+$) neurons. $n = 4$ animals. All quantitative data presented as bar graphs in means ± SEM and evaluated by one-way ANOVA and Tukey's post hoc multiple comparisons. Nonsignificant comparisons are not identified. $^*P < 0.05$, $^{**}P < 0.01$, $^{***}P < 0.001$, $^{****}P < 0.0001$.

suggested that the CHI3L1–CRTH2–GSK-3β/β-catenin pathway can be targeted to rescue the impaired neurogenesis in the context of neuroinflammation.

Last, we examined the translational potential in targeting this identified CHI3L1 signaling mechanism by exploring the growing list of CRTH2 antagonists, a promising class of anti-inflammatory drugs in multiple clinical trials already (*63*). To test the feasibility, we chose the compound AZD1981 (AstraZeneca, Gothenburg, Sweden) (*64*), a potent, selective, and noncompetitive CRTH2 antagonist that went through a phase 2b study as an adjuvant for asthma therapy (*65*). For the in vitro neurogenesis assay, we stimulated cultured NSCs with vehicle control PBS or CHI3L1, with or without coincubation of AZD1981 (Fig. 7E). The AZD1981 treatment alone did not alter the basal level of NSC proliferation; it nevertheless offset the suppression of proliferation by CHI3L1 and sustained the number of proliferating cells as in the control PBS conditions (Fig. 7F). Along the in vitro neuronal differentiation process, cultured NSCs treated with AZD1981 were insensitive to the CHI3L1 stimulation and still able to differentiate into neurons to the extent of their control counterparts (Fig. 7G). Next, we turned to our established settings of chronic msAQP4-IgG perfusion and labeling with BrdU and EdU to evaluate the functional output of AZD1981 in vivo. Given the great tolerance (*65*), the mice were dosed with AZD1981 at the higher range of 1 mg/kg or with just vehicle dimethyl sulfoxide (DMSO) as the control by daily intraperitoneal injection for 4 weeks (Fig. 7H). We found that AZD1981 relieved the repression of neurogenesis in the neuroinflammatory condition initiated by msAQP4-IgG perfusion: In msAQP4-IgG groups (msAQP4-IgG alone and msAQP4-IgG + AZD1981), AZD1981-treated mice had significantly more proliferating cells (Fig. 7I) that were radial glia–like NSCs (Fig. 7J) and had also more newborn neurons that were either immature (Fig. 7K) or mature (Fig. 7L). The rescue of neuronal differentiation was indeed partial (Fig. 7, K and L), which was anticipated considering that the pharmacological blockade of CRTH2 would not be complete due to the suboptimal efficiency of AZD1981 in crossing the blood-brain barrier (*64*). In summary, these results of genetic knockdown or pharmacological blockade demonstrated that the CRTH2 receptor could be targeted to shut down the CHI3L1 signaling that adversely affects hippocampal neurogenesis and function after astroglial activation in neuroinflammation.

DISCUSSION

Neuroinflammation, a process executed by activation of astrocytes (*46*), is now the major therapeutic target for an array of brain diseases ranging from cancers (e.g., glioblastoma) (*66*), neurodegeneration (*2*), and autoimmune disorders such as multiple sclerosis (*67*) and NMO (*48*). Uncovering the molecular determinant for the inflammatory neurotoxicity after astroglial activation is thus of tremendous translational potential for the development of next-generation anti-neuroinflammatory treatments. In this study, we demonstrated that astrocyte-secreted CHI3L1 is the main effector of the astroglial activation for the compromised hippocampal function in neuroinflammation. By using multiple model systems with activated astrocytes and CHI3L1 induction, we showed that CHI3L1 drives the neurogenic and cognitive defects in neuroinflammation. Specifically, CHI3L1 interacts with the receptor CRTH2 on NSCs and triggers a downstream signaling pathway mediated by GSK-3β and β-catenin to inhibit the process of adult hippocampal neurogenesis. Blocking this CHI3L1–CRTH2–GSK-3β/β-catenin cascade with genetic knockout and knockdown or pharmacological blockade could restore the hippocampal neurogenesis and cognitive function. In summary, our findings provided a fresh insight into CHI3L1′s role in the brain, substantially expanding the functionality repertoire from being a neuroinflammatory disease marker to a maker and also to an alternative therapeutic target for a much-needed therapy.

As the cognitive decline arising from inflammatory immune responses constitutes a fair share of disease burden in brain disorders like the NMO, its underlying mechanism is still inadequately understood but has been heavily linked to the adult hippocampal neurogenesis. While the situation remains unsettled in human brains, the adult-born neurons in rodents and nonhuman primates apparently contribute to the structural and functional plasticity of the hippocampus (*68*–*70*) and to the performance of several cognitive tasks, including spatial learning and memory and the pattern separation that is associated to the DG function in humans (*71*). Neurogenesis in the adult hippocampus is tightly controlled by the environmental cues within the SGZ, and an inflammatory milieu prohibits NSC proliferation and differentiation (*29*–*31*). Our findings thus support that CHI3L1 acts in a paracrine fashion and disturbs the neurogenic niche for NSCs in neuroinflammation. One caveat is that while CHI3L1 is essential for the inhibitory effect from astrocyte activation, other glial factors, the proinflammatory cytokines we showed earlier for example, would modulate the microenvironment of SGZ by affecting other cell types but might be left undetected due to our concentration on the intrinsic responses of NSCs. Regardless, the signaling mechanism delineated here still serves as a pioneering piece of knowledge for the CHI3L1 biology in the brain.

Among the scarce relevant literature, CHI3L1 was recently reported to be induced in astrocytes activated by genetic disruption of circadian rhythm; in this form of astroglial activation, CHI3L1 knockout hampered the accumulation of amyloid pathology in a transgenic mouse strain of Alzheimer′s disease, likely through the restoration of phagocytic clearance in the diseased brains (*11*). This notable publication, in conjunction with our study, substantiated the neurotoxic effect of CHI3L1 and highlighted the potential benefit of targeting the CHI3L1 receptor pathway. Our discovery of CRTH2 as the NSC CHI3L1 receptor was a surprise to us. CRTH2 was initially identified as a G protein–coupled receptor expressed on human T_H2 cells (*72*), and its activation leads to leukocyte chemotaxis in the development of allergic responses (*73*, *74*). To date, little is known about the expression and function of CRTH2 in CNS. One group reported that CRTH2 knockout in mice attenuated the LPS-induced decreases in social interaction and novel exploratory behavior with a yet-to-be-elucidated mechanism and proposed that central CRTH2 signaling can mediate cognitive function (*75*). The fact that CRTH2 is indeed the second identified receptor for prostaglandin D2 (*76*), however, represents a limitation in interpreting our in vivo results on blocking CRTH2 activation. In vitro, we used the shRNA against CRTH2 and the selective CRTH2 antagonist AZD1981 to firmly establish the ligand-receptor relationship for CHI3L1-CRTH2. In vivo, both approaches intended to block CRTH2 activation by CHI3L1 binding also potentially obstructed the prostaglandin D2 signaling, which is involved in a wide variety of neurophysiological functions

(*77*), and, in the unusual context of neuronal differentiation, was counterintuitively described to be able to promote outgrowth of neuronal processes in immortalized neuronal cells via an unidentified receptor (*78*). While we could not verify such antagonizing effect of prostaglandin D2 in our NSCs, our findings on CRTH2 blocking solidly suggested that, at least in an inflammatory condition, CRTH2 is predominantly activated by CHI3L1 to mediate the inhibition of neurogenesis. Our identification of the specific signaling mechanism therefore encourages the medical attempts for amending or even reversing the hippocampal dysfunctions provoked by CHI3L1 in neuroinflammation.

Last, the clinical translation of our discovery would be straightforward, given the abundance in the existing options for the repurposing. A class of selective CRTH2 antagonists including AZD1981 has been rigorously tested in multiple clinical trials mostly for allergy (*65*) and is proven to have great tolerance, high bioavailability, and decent anti-inflammatory efficacy. Moreover, a few of these compounds were specifically designed for optimal CNS penetration (*79*, *80*) and therefore are well poised to treat neuroinflammation. There has been an evolving interest in developing therapeutic strategies aimed to enhance endogenous neurogenesis in some pathological conditions of cognitive impairments such as aging and Alzheimer′s disease (*81*–*83*). This interest would be escalated after this study and future works focusing on this topic, considering the common CHI3L1 induction observed in scores of neurological disorders hallmarked by inflammatory pathology. Accordingly, the impact of developing a therapy targeting the inhibitory CHI3L1 signaling to improve neurogenesis and cognitive function is anticipated to be far-reaching.

MATERIALS AND METHODS

Study design

This study was designed to thoroughly investigate the neurobiological role of CHI3L1/YKL-40, which is secreted by activated astrocytes, in the neurogenic and cognitive dysfunctions caused by neuroinflammation. The study aimed to inspire an alternative translational approach for CNS disorders characterized by CHI3L1 induction and immune responses. The study used in vitro cellular models, in vivo mouse models, and clinical samples to find a CHI3L1 signaling mechanism that activates the CRTH2 receptor and downstream GSK-3β/β-catenin signaling cascade, thus governing hippocampal neurogenesis and function. The study also demonstrated that this CHI3L1 signaling can be targeted to mitigate the detrimental effects of neuroinflammation. The research involves the characterization of CHI3L1 induction and inflammatory features in mouse astrocyte cultures, the demonstration of CHI3L1′s inhibitory effects on the proliferation and neuronal differentiation of NSCs, and the correlation between CHI3L1 secretion and neurocognitive impairment and hippocampal dysfunction in patients with NMO. Mouse models of CHI3L1 overexpression and primary astrocytopathy were created to reveal the inhibitory effects of CHI3L1 on adult hippocampal neurogenesis and learning and memory behaviors. Furthermore, the study demonstrated that astrocyte-specific CHI3L1 depletion and blockade of CRTH2 receptor activation rescue the neurogenic and cognitive deficits caused by the inflammatory microenvironment of the hippocampus. The study followed rigorous experimental protocols including at least three independent experiments as biological replicates, random assignment of experimental units to groups, blinded analysis, and adherence to institutional guidelines for animal care. The International Committee of Medical Journal Editors (ICMJE) guidelines were followed. The clinical study enrolled 73 patients and 46 age-matched healthy control NMO patients who meet diagnostic criteria (*84*), and data are collected from them during the recovery stage, with no clinical deterioration, at least 3 months from the end of attack or relapse. Written informed consent was obtained from all participants.

Primary astrocyte culturing and treatments for the collection of ACM

The isolation and primary culturing of mouse astrocytes were performed as described by us previously (*85*, *86*), with the procedures being included in the Supplementary Materials. The cultures were treated with controls or biological reagents at the indicated final concentration for the described experimental durations: Dulbecco′s PBS (as the vehicle), IL-1β (10 ng/ml; 200-01B, PeproTech), monoclonal mouse antibodies targeting AQP4 (msAQP4-IgG, 100 ng/ml), control mouse IgG (100 ng/ml), purified human autoantibodies against AQP4 (hsAQP4-IgG, 100 ng/ml), and control human IgG (100 ng/ml). The acquisition of mouse and human antibodies was detailed in the following section. The primary astrocyte cultures were harvested by fixation with 4% paraformaldehyde (PFA) for immunostaining and by lysis buffers for RNA sequencing (RNA-seq) and qPCR assays.

To collect the ACM (Fig. 2, J to O), the primary mouse astrocyte cultures were first treated with hsCtrl-IgG or hsAQP4-IgG at 100 ng/ml for 24 hours. The ACM were harvested and filtered with 0.22-μm nylon mesh (BS-QT-037, Biosharp). To remove the astrocyte-secreted CHI3L1, the filtered ACM were added with the anti-CHI3L1 monoclonal antibodies (rabbit, Proteintech) or msCtrl-IgG at 100 ng/ml plus protein A beads (71149800, GE Healthcare), tumbled for 4 hours at 4°C, and centrifuged to clear the IgG contents. The cleared ACM was then supplemented with factors to constitute the culture media for the proliferation or neuronal differentiation of cultured mouse NSCs. The purified mouse NSCs were cultured in ACM-based proliferation medium for 3 days. On day 3, half of the cultures were subject to EdU labeling for 2 hours before the fixation and immunostaining to evaluate the proliferation. Half of the cultures were changed with the ACM-based differentiation media to initiate the neuronal differentiation and 3 days later were fixed and immunostained for confocal analyses of neuronal differentiation.

Primary mouse NSC isolation, culturing, and in vitro differentiation

The mouse NSCs used in this study were purified from living DG tissues acutely dissected from 8-week young adult wild-type C57BL/6 mice, largely based on the protocol published by Guo *et al.* (*50*). The procedures of NSC in vitro differentiation were described in detail in the Supplementary Materials. In brief, the NSC cultures were cultured in the proliferation medium for 3 days for the assays of proliferation (by EdU labeling) and then grown in the differentiation medium for additional 3 days for the assessment of neuronal differentiation (by the expression of neuronal and glial markers). The following reagents were added to the proliferating or differentiating NSC cultures: vehicle control PBS or recombinant CHI3L1 protein (100 ng/ml; 2599-CH-050, R&D Systems), CCL7

(100 ng/ml; P4424, Abnova), CXCL1 (100 ng/ml; P04800, Solarbio), GBP5 (100 ng/ml; P04632, Solarbio), ISG15 (100 ng/ml; P02878, Solarbio), VCAM1 (100 ng/ml; P05662, Solarbio), C3 (100 ng/ml; P02621, Solarbio), IL-1α (100 ng/ml; PRP1021, Abbkine), or IL-1β (100 ng/ml; PRP1019, Abbkine). The treated cultures were harvested by fixation with 4% PFA and then subjected to immunostaining for confocal imaging of the EdU or BrdU expression, in conjunction with neural or nuclear markers.

Human and mouse IgG acquisition

The hybridoma cell line producing monoclonal mouse IgG specifically recognizing the mouse AQP4 extracellular domain (clone E5415B; hereafter referred to as msAQP4-IgG) was provided by Y. Abe at the Keio University, Tokyo, Japan. These antibodies were described in detail by Miyazaki-Komine *et al.* (*39*) and are also commercially available (MABN2526-25UG, Sigma-Aldrich). The control mouse IgG was the normal mouse IgG validated for use in immunoprecipitation and immunoblotting (12–371, Sigma-Aldrich). The human autoantibodies against AQP4 (hsAQP4-IgG) were purified from the pooled plasma samples of anti-AQP4 seropositive NMO patients (hsAQP4-IgG) or healthy volunteers (hsCtrl-IgG) undergoing plasma exchange using protein A beads (71149800, GE Healthcare). The beads were eluted with 100 mM glycine HCl (pH 2.5), and then the eluent was concentrated using an Amicon Ultra 15 centrifugal filtration unit (100 kDa, Millipore, Billerica, MA). The concentration of IgG was 0.22 μM, and the working portion was kept at −80°C. The purification of hsAQP4-IgG and hsCtrl-IgG was repeated for three times from three independent batches of pooled sera.

Immunofluorescence staining of NSC proliferation and differentiation

For in vitro experiments, primary cultures of mouse astrocytes or NSCs were fixed with 4% PFA for 40 min, followed by washing in PBS. Then, the cells were blocked with donkey serum (300 μl/10 ml) and 10% Triton X-100 (250 μl/10 ml) for 1 hour at room temperature and sequentially incubated with primary antibodies overnight at 4°C. The cells were washed with PBS three times, and then the cells were incubated with the secondary antibody at room temperature for 1 hour. The nuclei were then stained with 4′,6-diamidino-2-phenylindole (DAPI) and observed under a laser confocal microscope. Each group of immunohistochemical experiments was repeated at least three times. The following primary antibodies were used: chicken anti-GFAP (1:1000, Abcam), mouse anti-Tuj1 (1:1000, Abcam), mouse anti–IL-13Rα2 [1:500, Cell Signaling Technology (CST)], rabbit anti-CHI3L1 (1:1000, Invitrogen), rabbit anti-CRTH2 (1:500, Invitrogen), and rabbit anti-TMEM219 (1:500, CST). The following fluorescent secondary antibodies were used: goat anti-mouse 488, goat anti-mouse 568, goat anti-mouse 647, goat anti-rabbit 488, goat anti-rabbit 568, goat anti-rabbit 647, and goat anti-chicken 647.

RNA isolation, qPCR, and genome-wide RNA-seq

mRNA from mouse hippocampal tissue or primary astrocytes was extracted with a miRNeasy kit (Qiagen). Then, mRNA was quantified and checked for purity using a NanoDrop spectrophotometer (Thermo Fisher Scientific). The cDNA was converted from 1 μg of mRNA using the SureScript First-Strand cDNA Synthesis Kit (Genecopoeia Company). Reverse transcription qPCR was performed using BlazeTaq SYBR Green qPCR Mix (Genecopoeia Company) with Applied Biosystems (Thermo Fisher Scientific). Fold changes were calculated as $2^{-\Delta\Delta CT}$ with glyceraldehyde-3-phosphate dehydrogenase (GAPDH) used as the endogenous control. The sequences of the primers for the individual genes of interest were included in the Supplementary Materials. The RNA-seq was performed by using the Illumina HiSeq 2500 system. The transcriptomic changes induced by AQP4 autoantibodies were plotted by gene fold changes on a $\log_2$ scale and comparing between three biological replicates of the hsCtrl-IgG and hsAQP4-IgG treatments after normalization to the average of three replicates of the untreated astrocytes from the same batches of cultures ($\log_2 0 = 1.0$; Fig. 1, E to J). This approach of normalization was intended to unmask the general effect of the hsCtrl-IgG treatment.

Immunoblotting and the densitometric analysis

The procedures are described in the Supplementary Materials. The primary antibodies used were rabbit anti-CHI3L1 (1:1000, Abcam), rabbit anti-CRTH2 (1:1000, Invitrogen), mouse anti-TMEM219 (1:1000, Abcam), rabbit anti–IL-13Rα2 (1:1000, Biorbyt), rabbit anti–GSK-3β (1:1000, Bioss), rabbit anti–p-GSK-3β (1:1000, CST), rabbit anti–β-catenin (1:1000, CST), and mouse anti–β-actin (1:1000, Huabio). β-Actin was used as the loading control. The intensity of the bands was quantified using ImageJ software.

The ELISA for CHI3L1 levels

The ELISA samples included human serum, human CSF, the ACM, and the lysates of freshly dissected mouse hippocampal tissues. Blood samples with the anticoagulant heparin added were first spun for 15 min at 8000 rpm at 4°C, and the supernatant serum was then collected. Levels of CHI3L1 in serum or CSF were measured with commercial ELISA kits (R&D Systems, MN, USA) based on the provided instructions, including the generation of a standard curve based on a series of dilution of CHI3L1 proteins. Levels of CHI3L1 were measured with commercial ELISA kits (MEIMIAN, MM-44752M2). The absorbance of each standard and sample was measured at 450 nm.

Production of lentivirus and AAV particles

The lentivirus and AAV preparations were routinely produced as we described previously (*85*, *86*), with the procedures being included in the Supplementary Materials. For the in vitro lentiviral transductions, we calculated the amount of virus preparations to deliver the multiplicity of infection (MOI) of 5 to 10 in primary cultures of mouse astrocytes and NSCs. For the stereotaxic injections in vivo, the virus preparations were concentrated by ultracentrifugation to achieve the concentration of 10^8 to 10^9 as indicated in figure legends. The sequences of the validated shRNAs against the tested CHI3L1 receptors are included in the Supplementary Materials.

EdU and BrdU administration for confocal analyses of NSC proliferation and differentiation

For analysis of NSC proliferation and neuronal differentiation in the adult mouse hippocampal DG, adult mice were intraperitoneally injected EdU (100 mg/kg) and sacrificed 2 hours after injection, and then the EdU Cell Proliferation Kit was used according to the manufacturer′s protocol (C0078L, Beyotime). For analysis of cell differentiation in the adult mouse hippocampal DG, adult mice were

intraperitoneally injected BrdU (100 mg/kg) for 4 days and sacrificed at the fourth week after injection. Immunofluorescence staining and quantification of $BrdU^+$ cells in the SGZ and granulosa cell layers were performed largely as the standardized method described by Zhao and van Praag (*55*), in which two-dimensional (2D) confocal images were reconstructed into a 3D rendition to calculate the volume of DG for a more stable spatial reference for the quantification. For quantification of cells expressing stage-specific markers, 1 in 12 serial sections starting at the beginning of the hippocampus (relative to bregma, 1.5 mm) to the end of the hippocampus (relative to bregma, 3.5 mm) was used. Quantification of EdU^+ or $BrdU^+$ cells and phenotypic quantification of EdU^+ or $BrdU^+$ cells (double labeling with Sox2, GFAP, DCX, and NeuN) in the granule layer were performed using a Leica confocal microscope in at least three sections containing the DG from at least three different animals. The value of *n* is described in the figure legends.

TWS119 and AZD1981 administration

TWS119 (HY-10590, MedChem Express) is a highly effective inhibitor of GSK-3β, belonging to the disubstituted pyrrolopyrimidine class. It has a median inhibitory concentration (IC_{50}) value of 30 nM and a dissociation constant (K_d) value of 126 nM (*61*). AZD1981 (M04757, BJBALB Co. Ltd.) was administered by intraperitoneal injections at the dosage of 1 mg/kg every other day for 4 weeks. AZD1981 was documented to exhibit cross-species binding activity to CRTH2 and block the activation of eosinophils in mice, rats, guinea pigs, rabbits, and dogs. In clinical trials, it was well tolerated and no safety concerns were identified.

Stereotaxic injections of IgG, lentivirus, and AAV into the hippocampus

The surgical procedures were regularly executed by the protocols described previously by the investigators. Roughly 8-week-old C57BL/6 or *Chil1*$^{f/f}$ mice were anesthetized by the inhalation of isoflurane delivered by a mask (2% gas in air mixture) and fixed on a stereotaxic frame (RWD Life Science, Shenzhen, China). One microliter of virus preparation with a titer greater than 5×10^8/ml was injected into the DG of the hippocampus. The infusion needle was stereotaxically implanted into the DG using the following coordinates relative to bregma: caudal side: −2.0 mm; transverse direction: ±1.7 mm; ventral: −1.9 mm. All mice were ambulating normally after awakening from anesthesia.

Mini-osmotic pump (mini-pump) implementation and IgG infusion

The procedures of implementing the mini-pump for intrahippocampal infusion were described in detail by the researchers. In short, the components of the osmotic pumps were first assembled according to the manufacturer's instructions (ALZET, model 1002). The mini-osmotic pump was then filled with msCtrl-IgG or msAQP4-IgG (1 μg/100 μl in PBS) and then positioned at the following coordinates relative to bregma: caudal side: −2.0 mm; transverse direction: ±1.7 mm; ventral: −1.9 mm. The infusion flow rate was set at 0.25 μl/hour for 14 days.

Immunohistochemistry for confocal imaging of mouse hippocampal slices

The procedures are described in the Supplementary Materials. The primary antibodies used were mouse anti-GFAP (1:1000, CST), rabbit anti-GFAP (1:1000, CST), chicken anti-GFAP (1:1000, Abcam), rabbit anti-NeuN (1:500, Abcam), mouse anti-DCX (1:200, Santa Cruz Biotechnology), rabbit anti-Sox2 (1:500, Abcam), mouse anti-Sox2 (1:500, Abcam), rat anti-BrdU (1:1000, Abcam), mouse anti-Tuj1 (1:1000, Abcam), rabbit anti–IIL-13Rα2 (1:500, CST), rabbit anti-CHI3L1 (1:500, Abcam), goat anti-CHI3L1 (1:500, R&D Systems), rabbit anti-CHI3L1 (1:500, Solarbio), rabbit anti-CRTH2 (1:500, Invitrogen), mouse anti-CRTH2 (1:500, Invitrogen), and mouse anti-TMEM219 (1:500, CST). The following fluorescent secondary antibodies were used: goat anti-mouse 488, goat anti-mouse 568, goat anti-mouse 647, goat anti-rabbit 488, goat anti-rabbit 568, goat anti-rabbit 647, goat anti-rat 568, and goat anti-chicken 647. Confocal single plane images and z stacks were taken with a laser confocal microscope (Leica, TCS SP8) equipped with four laser lines (405, 488, 568, and 647 nm) and 63×, 40×, and 20× objective lenses.

Animal care and behavioral assays

The routine animal care and behavioral paradigms of OFT and MWM were performed largely as described by Wang *et al.* (*35*), with the procedures being described in the Supplementary Materials. All animal procedures were performed in accordance with the National Institutes of Health *Guide for the Care and Use of Laboratory Animals* and were approved by the Animal Care Committee and the Ethics Committee of the Third Affiliated Hospital of Sun Yat-sen University.

Clinical data collection

NMO patients were diagnosed based on the 2015 International Panel for NMO Diagnosis (IPND) criteria (*84*) and received treatments and follow-up cares at the Third Affiliated Hospital of Sun Yat-sen University and the Second Affiliated Hospital of Guangzhou Medical University. Blood and CNS samples, MRI scans, and neuropsychological assessments were acquired during a clinically stable stage when the patients were recovering from the attack or relapse for at least 3 months did not show symptomatic deterioration. For all the individuals who participated in our clinical study, the informed consent was obtained after the nature and possible consequences of the study were explained. This study was approved by the Ethics Committee of the Third Affiliated Hospital of Sun Yat-sen University, in strict accordance with the Declaration of Helsinki.

Human brain samples

Frozen sections of human brain were obtained from biopsy brain tissues of one AQP4-IgG serum-positive NMO patient and one control. The clinical characteristic data of the pathological specimen providers are shown in table S3, and other details were reported in our prior studies (*33*, *49*).

MRI acquisition and hippocampal subfield volume analysis

All MRI data were obtained on a 3.0-T magnetic resonance system (Philips Medical System Ingenia scanner) with dStream head coil. Structural images of the whole brain were scanned using 3D fast spoiled gradient-echo sequence. FLAIR data were scanned using a repetition time of 7000 ms, a flip angle of 90°, an echo time of 125 ms, an acquisition matrix of 272 × 176, and a and slice thickness of 6 mm. First, the whole hippocampus was automatically segmented and calculated using FreeSurfer version 7.1.1, and the hippocampal

subfields were automatically segmented and measured using a package available. Using this algorithm, the hippocampus was accurately segmented into the following subfields: parasubiculum, presubiculum, subiculum, CA1, CA2/3, CA4, granular cell layer of DG, hippocampus-amygdala transition area, fimbria, molecular layer, fissure, and hippocampal tail.

Clinical screening

We recorded the demographic and clinical information of all patients, which included age, sex, education, and disease duration. MMSE, SDMT, and BVMT-R can comprehensively, accurately, and quickly reflect the subjects' mental state and the degree of cognitive impairment. CVLT assessed the subjects' learning and memory abilities, including immediate recall (trials 1 to 5, T1-5), short delayed free recall (SDFR), short delayed cue recall (SDCR), long delayed cue recall (LDCR), and long delayed free recall (LDFR). General anxiety and depression-relevant behaviors were assessed using HARS and HDRS, respectively. Behavioral symptoms were assessed via interview with the informant and quantified using the Frontal Behavioral Inventory.

Statistical analysis

The sample size was not predetermined by any statistical methods as the effect sizes were unavailable before the experiments. The samples sizes were all described in the figure legends. No exclusion criteria were preestablished. The normality of the data distribution was routinely determined by a Shapiro-Wilk normality test ($P < 0.05$ indicating a nonnormal distribution). For the data confirmed to be normally distributed data, we used Student's t test for pairwise comparisons and one-way or two-way analysis of variance (ANOVA) followed by Tukey's post hoc test for three groups or more, as indicated in the figure legends. For data that are not normally distributed, nonparametric alternatives, such as Mann-Whitney or Kruskal-Wallis tests, were used. $P < 0.05$ is considered to be statistically significant. All data in bar graphs and summary plots were shown as means ± SEM of at least three independent biological replicates in all figures. Descriptive statistics were used to examine the demographic characteristics, information, and neuropsychological testing of patients. In addition, the correlation between the neuropsychological testing and the CHI3L1 level was performed using the Pearson correlation coefficient. Significance was reported as $^{*}P < 0.05$, $^{**}P < 0.01$, $^{***}P < 0.001$, and $^{****}P < 0.0001$. All statistical analyses were performed in GraphPad Prism 9 (GraphPad Software).

Supplementary Materials

This PDF file includes:

Supplementary Materials and Methods
Figs. S1 to S7
Tables S1 to S3
Legend for data file S1
References

Other Supplementary Material for this manuscript includes the following:

Data file S1

REFERENCES AND NOTES

1. T. Zhao, Z. Su, Y. Li, X. Zhang, Q. You, Chitinase-3 like-protein-1 function and its role in diseases. *Signal Transduct. Target. Ther.* **5**, 201 (2020).
2. K. Connolly, M. Lehoux, R. O'Rourke, B. Assetta, G. A. Erdemir, J. A. Elias, C. G. Lee, Y.-W. A. Huang, Potential role of chitinase-3-like protein 1 (CHI3L1/YKL-40) in neurodegeneration and Alzheimer's disease. *Alzheimers Dement.* **19**, 9–24 (2023).
3. C. G. Lee, C. A. Da Silva, C. S. Dela Cruz, F. Ahangari, B. Ma, M. J. Kang, C. H. He, S. Takyar, J. A. Elias, Role of chitin and chitinase/chitinase-like proteins in inflammation, tissue remodeling, and injury. *Annu. Rev. Physiol.* **73**, 479–501 (2011).
4. S. Kamle, B. Ma, C. H. He, B. Akosman, Y. Zhou, C.-M. Lee, W. S. El-Deiry, K. Huntington, O. Liang, J. T. Machan, M.-J. Kang, H. J. Shin, E. Mizoguchi, C. G. Lee, J. A. Elias, Chitinase 3-like-1 is a therapeutic target that mediates the effects of aging in COVID-19. *JCI Insight* **6**, e148749 (2021).
5. E. J. Kwak, J. Y. Hong, M. N. Kim, S. Y. Kim, S. H. Kim, C. O. Park, K. W. Kim, C. G. Lee, J. A. Elias, H. M. Jee, M. H. Sohn, Chitinase 3-like 1 drives allergic skin inflammation via Th2 immunity and M2 macrophage activation. *Clin. Exp. Allergy* **49**, 1464–1474 (2019).
6. C. G. Lee, D. Hartl, G. R. Lee, B. Koller, H. Matsuura, C. A. Da Silva, M. H. Sohn, L. Cohn, R. J. Homer, A. A. Kozhich, A. Humbles, J. Kearley, A. Coyle, G. Chupp, J. Reed, R. A. Flavell, J. A. Elias, Role of breast regression protein 39 (BRP-39)/chitinase 3-like-1 in Th2 and IL-13-induced tissue responses and apoptosis. *J. Exp. Med.* **206**, 1149–1166 (2009).
7. C.-M. Lee, C. H. He, A. M. Nour, Y. Zhou, B. Ma, J. W. Park, K. H. Kim, C. Dela Cruz, L. Sharma, M. L. Nasr, Y. Modis, C. G. Lee, J. A. Elias, IL-13Rα2 uses TMEM219 in chitinase 3-like-1-induced signalling and effector responses. *Nat. Commun.* **7**, 12752 (2016).
8. D. Low, R. Subramaniam, L. Lin, T. Aomatsu, A. Mizoguchi, A. Ng, A. K. DeGruttola, C. G. Lee, J. A. Elias, A. Andoh, M. Mino-Kenudson, E. Mizoguchi, Chitinase 3-like 1 induces survival and proliferation of intestinal epithelial cells during chronic inflammation and colitis-associated cancer by regulating S100A9. *Oncotarget* **6**, 36535–36550 (2015).
9. H. T. Tran, I. A. Lee, D. Low, A. Kamba, A. Mizoguchi, H. N. Shi, C. G. Lee, J. A. Elias, E. Mizoguchi, Chitinase 3-like 1 synergistically activates IL6-mediated STAT3 phosphorylation in intestinal epithelial cells in murine models of infectious colitis. *Inflamm. Bowel Dis.* **20**, 835–846 (2014).
10. Y. Zhou, H. Peng, H. Sun, X. Peng, C. Tang, Y. Gan, X. Chen, A. Mathur, B. Hu, M. D. Slade, R. R. Montgomery, A. C. Shaw, R. J. Homer, E. S. White, C. M. Lee, M. W. Moore, M. Gulati, C. G. Lee, J. A. Elias, E. L. Herzog, Chitinase 3-like 1 suppresses injury and promotes fibroproliferative responses in mammalian lung fibrosis. *Sci. Transl. Med.* **6**, 240ra276 (2014).
11. B. V. Lananna, C. A. McKee, M. W. King, J. L. Del-Aguila, J. M. Dimitry, F. H. G. Farias, C. J. Nadarajah, D. D. Xiong, C. Guo, A. J. Cammack, J. A. Elias, J. Zhang, C. Cruchaga, E. S. Musiek, Chi3l1/YKL-40 is controlled by the astrocyte circadian clock and regulates neuroinflammation and Alzheimer's disease pathogenesis. *Sci. Transl. Med.* **12**, eaax3519 (2020).
12. L. Li, E. Tian, X. Chen, J. Chao, J. Klein, Q. Qu, G. Sun, G. Sun, Y. Huang, C. D. Warden, P. Ye, L. Feng, X. Li, Q. Cui, A. Sultan, P. Douvaras, V. Fossati, N. E. Sanjana, A. D. Riggs, Y. Shi, GFAP mutations in astrocytes impair oligodendrocyte progenitor proliferation and myelination in an hiPSC model of Alexander disease. *Cell Stem Cell* **23**, 239–251.e6 (2018).
13. J. Wurm, S. P. Behringer, V. M. Ravi, K. Joseph, N. Neidert, J. P. Maier, R. Doria-Medina, M. Follo, D. Delev, D. Pfeifer, J. Beck, R. Sankowski, O. Schnell, D. H. Heiland, Astrogliosis releases pro-oncogenic chitinase 3-like 1 causing MAPK signaling in glioblastoma. *Cancers (Basel)* **11**, 1437 (2019).
14. P. Muszynski, M. Groblewska, A. Kulczynska-Przybik, A. Kulakowska, B. Mroczko, YKL-40 as a potential biomarker and a possible target in therapeutic strategies of Alzheimer's disease. *Curr. Neuropharmacol.* **15**, 906–917 (2017).
15. C. L. Sutphen, M. S. Jasielec, A. R. Shah, E. M. Macy, C. Xiong, A. G. Vlassenko, T. L. Benzinger, E. E. Stoops, H. M. Vanderstichele, B. Brix, H. D. Darby, M. L. Vandijck, J. H. Ladenson, J. C. Morris, D. M. Holtzman, A. M. Fagan, Longitudinal cerebrospinal fluid biomarker changes in preclinical Alzheimer disease during middle age. *JAMA Neurol.* **72**, 1029–1042 (2015).
16. F. M. Iwamoto, A. F. Hottinger, S. Karimi, E. Riedel, J. Dantis, M. Jahdi, K. S. Panageas, A. B. Lassman, L. E. Abrey, M. Fleisher, L. M. DeAngelis, E. C. Holland, A. Hormigo, Serum YKL-40 is a marker of prognosis and disease status in high-grade gliomas. *Neuro Oncol.* **13**, 1244–1251 (2011).
17. S. Floro, T. Carandini, A. M. Pietroboni, M. A. De Riz, E. Scarpini, D. Galimberti, Role of chitinase 3-like 1 as a biomarker in multiple sclerosis: A systematic review and meta-analysis. *Neurol. Neuroimmunol. Neuroinflamm.* **9**, e1164 (2022).
18. Y. Qi, L. S. Chou, L. J. Zhang, M. Q. Liu, M. Yi, Q. X. Zhang, J. Wang, T. Li, D. Q. Zhang, L. Yang, Increased cerebrospinal fluid YKL-40 levels are associated with disease severity of neuromyelitis optica spectrum disorders. *Mult. Scler. Relat. Disord.* **45**, 102395 (2020).
19. J. Correale, M. Fiol, Chitinase effects on immune cell response in neuromyelitis optica and multiple sclerosis. *Mult. Scler.* **17**, 521–531 (2011).
20. L. Cubas-Núñez, S. Gil-Perotín, J. Castillo-Villalba, V. López, L. Solís Tarazona, R. Gasqué-Rubio, S. Carratalá-Boscá, C. Alcalá-Vicente, F. Pérez-Miralles, H. Lassmann, B. Casanova, Potential role of CHI3L1+ astrocytes in progression in MS. *Neurol. Neuroimmunol. Neuroinflamm.* **8**, e972 (2021).

21. V. A. Lennon, D. M. Wingerchuk, T. J. Kryzer, S. J. Pittock, C. F. Lucchinetti, K. Fujihara, I. Nakashima, B. G. Weinshenker, A serum autoantibody marker of neuromyelitis optica: Distinction from multiple sclerosis. *Lancet* **364**, 2106–2112 (2004).
22. D. Czarnecka, M. Oset, I. Karlinska, M. Stasiolek, Cognitive impairment in NMOSD—More questions than answers. *Brain Behav.* **10**, e01842 (2020).
23. E. Lopez-Soley, J. E. Meca-Lallana, S. Llufriu, Y. Blanco, R. Gomez-Ballesteros, J. Maurino, F. Perez-Miralles, L. Forero, C. Calles, M. L. Martinez-Gines, I. Gonzalez-Suarez, S. Boyero, L. Romero-Pinel, A. P. Sempere, V. Meca-Lallana, L. Querol, L. Costa-Frossard, M. Sepulveda, E. Solana, Cognitive performance and health-related quality of life in patients with neuromyelitis optica spectrum disorder. *J. Pers. Med.* **12**, 743 (2022).
24. L. Cacciaguerra, P. Valsasina, A. Meani, G. C. Riccitelli, M. Radaelli, M. A. Rocca, M. Filippi, Volume of hippocampal subfields and cognitive deficits in neuromyelitis optica spectrum disorders. *Eur. J. Neurol.* **28**, 4167–4177 (2021).
25. F. Zheng, Y. Li, Z. Zhuo, Y. Duan, G. Cao, D. Tian, X. Zhang, K. Li, F. Zhou, M. Huang, H. Li, Y. Li, C. Zeng, N. Zhang, J. Sun, C. Yu, X. Han, S. Hallar, F. Barkhof, Y. Liu, Structural and functional hippocampal alterations in multiple sclerosis and neuromyelitis optica spectrum disorder. *Mult. Scler.* **28**, 707–717 (2022).
26. Y. Liu, Y. Fu, M. M. Schoonheim, N. Zhang, M. Fan, L. Su, Y. Shen, Y. Yan, L. Yang, Q. Wang, N. Zhang, C. Yu, F. Barkhof, F. D. Shi, Structural MRI substrates of cognitive impairment in neuromyelitis optica. *Neurology* **85**, 1491–1499 (2015).
27. W. Qiu, A. G. Kermode, Brain MRI in neuromyelitis optica: What is its role? *Curr. Neurol. Neurosci. Rep.* **11**, 526–528 (2011).
28. R. Li, C. Li, Z. Mao, Q. Huang, Y. Shu, Y. Chang, J. Wang, Y. Wang, W. Qiu, Male patients with neuromyelitis optica spectrum disorders: Different clinical characteristics and worse steroid treatment response. *Neurol. Sci.* **42**, 3267–3274 (2021).
29. M. L. Monje, S. Mizumatsu, J. R. Fike, T. D. Palmer, Irradiation induces neural precursor-cell dysfunction. *Nat. Med.* **8**, 955–962 (2002).
30. M. L. Monje, H. Toda, T. D. Palmer, Inflammatory blockade restores adult hippocampal neurogenesis. *Science* **302**, 1760–1765 (2003).
31. C. T. Ekdahl, J. H. Claasen, S. Bonde, Z. Kokaia, O. Lindvall, Inflammation is detrimental for neurogenesis in adult brain. *Proc. Natl. Acad. Sci. U.S.A.* **100**, 13632–13637 (2003).
32. B. Asrican, J. Wooten, Y. D. Li, L. Quintanilla, F. Zhang, C. Wander, H. Bao, C. Y. Yeh, Y. J. Luo, R. Olsen, S. A. Lim, J. Hu, P. Jin, J. Song, Neuropeptides modulate local astrocytes to regulate adult hippocampal neural stem cells. *Neuron* **108**, 349–366.e6 (2020).
33. W. Luo, H. Xu, L. Xu, W. Jiang, C. Chen, Y. Chang, C. Liu, Z. Tian, X. Qiu, C. Xie, X. Li, H. Chen, S. Lai, L. Wu, Y. Cui, C. Tang, W. Qiu, Remyelination in neuromyelitis optica spectrum disorder is promoted by edaravone through mTORC1 signaling activation. *Glia* **71**, 284–304 (2023).
34. C. Tang, M. Wang, P. Wang, L. Wang, Q. Wu, W. Guo, Neural stem cells behave as a functional niche for the maturation of newborn neurons through the secretion of PTN. *Neuron* **101**, 32–44.e6 (2019).
35. J. Wang, Y. Cui, Z. Yu, W. Wang, X. Cheng, W. Ji, S. Guo, Q. Zhou, N. Wu, Y. Chen, Y. Chen, X. Song, H. Jiang, Y. Wang, Y. Lan, B. Zhou, L. Mao, J. Li, H. Yang, W. Guo, X. Yang, Brain endothelial cells maintain lactate homeostasis and control adult hippocampal neurogenesis. *Cell Stem Cell* **25**, 754–767.e9 (2019).
36. S. R. Hinson, I. C. Clift, N. Luo, T. J. Kryzer, V. A. Lennon, Autoantibody-induced internalization of CNS AQP4 water channel and EAAT2 glutamate transporter requires astrocytic Fc receptor. *Proc. Natl. Acad. Sci. U.S.A.* **114**, 5491–5496 (2017).
37. M. E. Walker-Caulfield, Y. Guo, R. K. Johnson, C. B. McCarthy, P. D. Fitz-Gibbon, C. F. Lucchinetti, C. L. Howe, NFκB signaling drives pro-granulocytic astroglial responses to neuromyelitis optica patient IgG. *J. Neuroinflammation* **12**, 185 (2015).
38. C. L. Howe, T. Kaptzan, S. M. Magana, J. R. Ayers-Ringler, R. G. LaFrance-Corey, C. F. Lucchinetti, Neuromyelitis optica IgG stimulates an immunological response in rat astrocyte cultures. *Glia* **62**, 692–708 (2014).
39. K. Miyazaki-Komine, Y. Takai, P. Huang, O. Kusano-Arai, H. Iwanari, T. Misu, K. Koda, K. Mitomo, T. Sakihama, Y. Toyama, K. Fujihara, T. Hamakubo, M. Yasui, Y. Abe, High avidity chimeric monoclonal antibodies against the extracellular domains of human aquaporin-4 competing with the neuromyelitis optica autoantibody, NMO-IgG. *Br. J. Pharmacol.* **173**, 103–114 (2016).
40. P. Hasel, I. V. L. Rose, J. S. Sadick, R. D. Kim, S. A. Liddelow, Neuroinflammatory astrocyte subtypes in the mouse brain. *Nat. Neurosci.* **24**, 1475–1487 (2021).
41. K. A. Guttenplan, M. K. Weigel, D. I. Adler, J. Couthouis, S. A. Liddelow, A. D. Gitler, B. A. Barres, Knockout of reactive astrocyte activating factors slows disease progression in an ALS mouse model. *Nat. Commun.* **11**, 3753 (2020).
42. J. L. Zamanian, L. Xu, L. C. Foo, N. Nouri, L. Zhou, R. G. Giffard, B. A. Barres, Genomic analysis of reactive astrogliosis. *J. Neurosci.* **32**, 6391–6410 (2012).
43. W. Luo, G. Pant, Y. K. Bhavnasi, S. G. Blanchard Jr., C. Brouwer, Pathview Web: User friendly pathway visualization and data integration. *Nucleic Acids Res.* **45**, W501–W508 (2017).
44. M. Kanehisa, The KEGG database. *Novartis Found. Symp.* **247**, 91–101 (2002).
45. A. Subramanian, P. Tamayo, V. K. Mootha, S. Mukherjee, B. L. Ebert, M. A. Gillette, A. Paulovich, S. L. Pomeroy, T. R. Golub, E. S. Lander, J. P. Mesirov, Gene set enrichment analysis: A knowledge-based approach for interpreting genome-wide expression profiles. *Proc. Natl. Acad. Sci. U.S.A.* **102**, 15545–15550 (2005).
46. S. A. Liddelow, B. A. Barres, Reactive astrocytes: Production, function, and therapeutic potential. *Immunity* **46**, 957–967 (2017).
47. H. Tang, Y. Sun, Z. Shi, H. Huang, Z. Fang, J. Chen, Q. Xiu, B. Li, YKL-40 induces IL-8 expression from bronchial epithelium via MAPK (JNK and ERK) and NF-κB pathways, causing bronchial smooth muscle proliferation and migration. *J. Immunol.* **190**, 438–446 (2013).
48. Y. Kim, S. Y. Kim, S.-M. Han, R. M. Payumo, K. Park, H. E. Kim, S.-H. Kim, J.-W. Hyun, E. Lee, H. J. Kim, Functional impairment of $CD19^{+}$ $CD24^{hi}$ $CD38^{hi}$ B cells in neuromyelitis optica spectrum disorder is restored by B cell depletion therapy. *Sci. Transl. Med.* **13**, eabk2132 (2021).
49. Y. Chang, W. Qiu, B. Zhang, D. He, H. Yang, Z. Lu, X. Hu, Analysis of two cases of Neuromyelitis Optica combined with tumefactive demyelinating lesions. *Chinese J. Neurol.* **47**, 163–167 (2014).
50. W. Guo, N. E. Patzlaff, E. M. Jobe, X. Zhao, Isolation of multipotent neural stem or progenitor cells from both the dentate gyrus and subventricular zone of a single adult mouse. *Nat. Protoc.* **7**, 2005–2012 (2012).
51. C. H. He, C. G. Lee, C. S. Dela Cruz, C. M. Lee, Y. Zhou, F. Ahangari, B. Ma, E. L. Herzog, S. A. Rosenberg, Y. Li, A. M. Nour, C. R. Parikh, I. Schmidt, Y. Modis, L. Cantley, J. A. Elias, Chitinase 3-like 1 regulates cellular and tissue responses via IL-13 receptor α2. *Cell Rep.* **4**, 830–841 (2013).
52. B. Ma, S. Kamle, C. He, C. Lee, J. A. Elias, Inhibition of melanoma lung metastasis by Chi3l1 neutralizing antibody. *Am. J. Respir. Crit. Care Med.* **197**, A5944 (2018).
53. C. Geis, C. Ritter, C. Ruschil, A. Weishaupt, B. Grünewald, G. Stoll, T. Holmoy, T. Misu, K. Fujihara, B. Hemmer, C. Stadelmann, J. L. Bennett, C. Sommer, K. V. Toyka, The intrinsic pathogenic role of autoantibodies to aquaporin 4 mediating spinal cord disease in a rat passive-transfer model. *Exp. Neurol.* **265**, 8–21 (2015).
54. L.-W. Yick, O. K.-F. Ma, R. C.-L. Ng, J. S.-C. Kwan, K.-H. Chan, Aquaporin-4 autoantibodies from neuromyelitis optica spectrum disorder patients induce complement-independent immunopathologies in mice. *Front. Immunol.* **9**, 1438 (2018).
55. X. Zhao, H. van Praag, Steps towards standardized quantification of adult neurogenesis. *Nat. Commun.* **11**, 4275 (2020).
56. C. Tang, W. Guo, Implantation of a mini-osmotic pump plus stereotactical injection of retrovirus to study newborn neuron development in adult mouse hippocampus. *STAR Protoc.* **2**, 100374 (2021).
57. Y. Zhou, C. H. He, E. L. Herzog, X. Peng, C. M. Lee, T. H. Nguyen, M. Gulati, B. R. Gochuico, W. A. Gahl, M. L. Slade, C. G. Lee, J. A. Elias, Chitinase 3-like-1 and its receptors in Hermansky-Pudlak syndrome-associated lung disease. *J. Clin. Invest.* **125**, 3178–3192 (2015).
58. D. C. Lie, S. A. Colamarino, H. J. Song, L. Désiré, H. Mira, A. Consiglio, E. S. Lein, S. Jessberger, H. Lansford, A. R. Dearie, F. H. Gage, Wnt signalling regulates adult hippocampal neurogenesis. *Nature* **437**, 1370–1375 (2005).
59. L. Xue, S. L. Gyles, A. Barrow, R. Pettipher, Inhibition of PI3K and calcineurin suppresses chemoattractant receptor-homologous molecule expressed on Th2 cells (CRTH2)-dependent responses of Th2 lymphocytes to prostaglandin D(2). *Biochem. Pharmacol.* **73**, 843–853 (2007).
60. A. Krishnankutty, T. Kimura, T. Saito, K. Aoyagi, A. Asada, S.-I. Takahashi, K. Ando, M. Ohara-Imaizumi, K. Ishiguro, S.-I. Hisanaga, In vivo regulation of glycogen synthase kinase 3β activity in neurons and brains. *Sci. Rep.* **7**, 8602 (2017).
61. S. Ding, T. Y. Wu, A. Brinker, E. C. Peters, W. Hur, N. S. Gray, P. G. Schultz, Synthetic small molecules that control stem cell fate. *Proc. Natl. Acad. Sci. U.S.A.* **100**, 7632–7637 (2003).
62. D. H. Kim, H. J. Park, S. Lim, J. H. Koo, H. G. Lee, J. O. Choi, J. H. Oh, S. J. Ha, M. J. Kang, C. M. Lee, C. G. Lee, J. A. Elias, J. M. Choi, Regulation of chitinase-3-like-1 in T cell elicits Th1 and cytotoxic responses to inhibit lung metastasis. *Nat. Commun.* **9**, 503 (2018).
63. R. Pettipher, T. T. Hansel, R. Armer, Antagonism of the prostaglandin D2 receptors DP1 and CRTH2 as an approach to treat allergic diseases. *Nat. Rev. Drug Discov.* **6**, 313–325 (2007).
64. T. Luker, R. Bonnert, S. Brough, A. R. Cook, M. R. Dickinson, I. Dougall, C. Logan, R. T. Mohammed, S. Paine, H. J. Sanganee, C. Sargent, J. A. Schmidt, S. Teague, S. Thom, Substituted indole-1-acetic acids as potent and selective CRTh2 antagonists-discovery of AZD1981. *Bioorg. Med. Chem. Lett.* **21**, 6288–6292 (2011).
65. E. D. Bateman, C. O'Brien, P. Rugman, S. Luke, S. Ivanov, M. Uddin, Efficacy and safety of the CRTh2 antagonist AZD1981 as add-on therapy to inhaled corticosteroids and long-acting β(2)-agonists in patients with atopic asthma. *Drug Des. Devel. Ther.* **12**, 1093–1106 (2018).
66. C. S. Malo, R. H. Khadka, K. Ayasoufi, F. Jin, J. E. AbouChehade, M. J. Hansen, R. Iezzi, K. D. Pavelko, A. J. Johnson, Immunomodulation mediated by anti-angiogenic therapy improves CD8 T cell immunity against experimental glioma. *Front. Oncol.* **8**, 320 (2018).
67. E. Quintana, C. Coll, J. Salavedra-Pont, M. Munoz-San Martin, R. Robles-Cedeno, J. Tomas-Roig, M. Buxo, C. Matute-Blanch, L. M. Villar, X. Montalban, M. Comabella, H. Perkal, J. Gich,

L. Ramio-Torrenta, Cognitive impairment in early stages of multiple sclerosis is associated with high cerebrospinal fluid levels of chitinase 3-like 1 and neurofilament light chain. *Eur. J. Neurol.* **25**, 1189–1191 (2018).
68. J. S. Snyder, N. Kee, J. M. Wojtowicz, Effects of adult neurogenesis on synaptic plasticity in the rat dentate gyrus. *J. Neurophysiol.* **85**, 2423–2431 (2001).
69. C. O. Lacefield, V. Itskov, T. Reardon, R. Hen, J. A. Gordon, Effects of adult-generated granule cells on coordinated network activity in the dentate gyrus. *Hippocampus* **22**, 106–116 (2012).
70. A. Marín-Burgin, L. A. Mongiat, M. B. Pardi, A. F. Schinder, Unique processing during a period of high excitation/inhibition balance in adult-born neurons. *Science* **335**, 1238–1242 (2012).
71. A. Bakker, C. B. Kirwan, M. Miller, C. E. L. Stark, Pattern separation in the human hippocampal CA3 and dentate gyrus. *Science* **319**, 1640–1642 (2008).
72. H. Abe, T. Takeshita, K. Nagata, T. Arita, Y. Endo, T. Fujita, H. Takayama, M. Kubo, K. Sugamura, Molecular cloning, chromosome mapping and characterization of the mouse CRTH2 gene, a putative member of the leukocyte chemoattractant receptor family. *Gene* **227**, 71–77 (1999).
73. T. Satoh, R. Moroi, K. Aritake, Y. Urade, Y. Kanai, K. Sumi, H. Yokozeki, H. Hirai, K. Nagata, T. Hara, M. Utsuyama, K. Hirokawa, K. Sugamura, K. Nishioka, M. Nakamura, Prostaglandin D2 plays an essential role in chronic allergic inflammation of the skin via CRTH2 receptor. *J. Immunol.* **177**, 2621–2629 (2006).
74. I. Spik, C. Brénuchon, V. Angéli, D. Staumont, S. Fleury, M. Capron, F. Trottein, D. Dombrowicz, Activation of the prostaglandin D2 receptor DP2/CRTH2 increases allergic inflammation in mouse. *J. Immunol.* **174**, 3703–3708 (2005).
75. R. Haba, N. Shintani, Y. Onaka, T. Kanoh, H. Wang, R. Takenaga, A. Hayata, H. Hirai, K. Y. Nagata, M. Nakamura, A. Kasai, R. Hashimoto, K. Nagayasu, T. Nakazawa, H. Hashimoto, A. Baba, Central CRTH2, a second prostaglandin D2 receptor, mediates emotional impairment in the lipopolysaccharide and tumor-induced sickness behavior model. *J. Neurosci.* **34**, 2514–2523 (2014).
76. H. Hirai, K. Tanaka, O. Yoshie, K. Ogawa, K. Kenmotsu, Y. Takamori, M. Ichimasa, K. Sugamura, M. Nakamura, S. Takano, K. Nagata, Prostaglandin D2 selectively induces chemotaxis in T helper type 2 cells, eosinophils, and basophils via seven-transmembrane receptor CRTH2. *J. Exp. Med.* **193**, 255–262 (2001).
77. M. S. Abdel-Halim, I. Lunden, G. Cseh, E. Änggård, Prostaglandin profiles in nervous tissue and blood vessels of the brain of various animals. *Prostaglandins* **19**, 249–258 (1980).
78. H. Nango, Y. Kosuge, N. Yoshimura, H. Miyagishi, T. Kanazawa, K. Hashizaki, T. Suzuki, K. Ishige, The molecular mechanisms underlying Prostaglandin D_2-induced neuritogenesis in motor neuron-like NSC-34 cells. *Cells* **9**, 934 (2020).
79. S. Ghosh, A. M. Elder, K. G. Carson, K. Sprott, S. Harrison, PGD2 receptor antagonists for the treatment of inflammatory diseases. World Patent WO2004032848 (2004).
80. L. Corradini, M. J. Field, R. A Kinloch, B. I. Williams-Jones, Method of treating neuropathic pain using a CRTH2 receptor antagonist. World Patent WO2005102338 (2005).
81. S. H. Choi, R. E. Tanzi, Is Alzheimer's disease a neurogenesis disorder? *Cell Stem Cell* **25**, 7–8 (2019).
82. B. W. Dulken, M. T. Buckley, P. Navarro Negredo, N. Saligrama, R. Cayrol, D. S. Leeman, B. M. George, S. C. Boutet, K. Hebestreit, J. V. Pluvinage, T. Wyss-Coray, I. L. Weissman, H. Vogel, M. M. Davis, A. Brunet, Single-cell analysis reveals T cell infiltration in old neurogenic niches. *Nature* **571**, 205–210 (2019).
83. L. K. Smith, Y. He, J. S. Park, G. Bieri, C. E. Snethlage, K. Lin, G. Gontier, R. Wabl, K. E. Plambeck, J. Udeochu, E. G. Wheatley, J. Bouchard, A. Eggel, R. Narasimha, J. L. Grant, J. Luo, T. Wyss-Coray, S. A. Villeda, β2-microglobulin is a systemic pro-aging factor that impairs cognitive function and neurogenesis. *Nat. Med.* **21**, 932–937 (2015).
84. D. M. Wingerchuk, B. Banwell, J. L. Bennett, P. Cabre, W. Carroll, T. Chitnis, J. de Seze, K. Fujihara, B. Greenberg, A. Jacob, S. Jarius, M. Lana-Peixoto, M. Levy, J. H. Simon, S. Tenembaum, A. L. Traboulsee, P. Waters, K. E. Wellik, B. G. Weinshenker; International Panel for NMO Diagnosis, International consensus diagnostic criteria for neuromyelitis optica spectrum disorders. *Neurology* **85**, 177–189 (2015).
85. Y.-W. A. Huang, B. Zhou, A. M. Nabet, M. Wernig, T. C. Sudhof, Differential signaling mediated by ApoE2, ApoE3, and ApoE4 in human neurons parallels Alzheimer's disease risk. *J. Neurosci.* **39**, 7408–7427 (2019).
86. Y.-W. A. Huang, B. Zhou, M. Wernig, T. C. Sudhof, ApoE2, ApoE3, and ApoE4 differentially stimulate APP transcription and Aβ secretion. *Cell* **168**, 427–441.e21 (2017).
87. D. Kaya, Z. Altun, E. Idiman, N. Karabay, S. Cevik, D. Arslan, Serum chitinase 3-like 1 levels in patients with multiple sclerosis and neuromyelitis optica (P5.271). *Neurology* **84**, P5.271 (2015).

Acknowledgments: We thank Y. Abe at the Keio University, Tokyo, Japan for providing the monoclonal mouse IgG targeting the extracellular domain of AQP4 (msAQP4-IgG, clone E5415B). We also thank W. Guo, Q. Wu, and Z. Lu for helpful discussions, and P. Lin and X. Han for technical assistance. **Funding:** This work was supported by the following: National Science Foundation of China grants 32100787 and 81771300 (C.T. and W.Q.), Science and Technology Plan Project of Guangzhou City grant 202201020489 (C.T.), National Key R&D Program of China grant 2022ZD0214300 (C.T.), and National Institutes of Health grants P20GM119943 (Y.-W.A.H.; subaward 7137296) and R21AG077697 (Y.-W.A.H.). **Author contributions:** Conceptualization: C.T., Y.-W.A.H., W.Q., and Y.C. Methodology: C.T., Y.C., W.Q., and Y.-W.A.H. Investigation: W.J., F.Z., H.X., L.X., Haoyang Li, Huilu Li, S.K.A., X.Y., S.L., X.Q., C.L., Y.W., and Y.L. Visualization: W.J., F.Z., H.X., X.Y., and K.C. Supervision: C.T., W.Q., Y.-W.A.H., Y.C., C.G.L., and J.A.E. Writing—original draft: Y.-W.A.H., C.T., W.Q., Y.C., W.J., and F.Z. Writing—review and editing: Y.-W.A.H., C.T., W.Q., and Y.C. **Competing interests:** J.A.E. is the Scientific Founder and a stock owner of Ocean Biomedical, which is focused on developing drugs based, in part, on the 18 glycosyl hydrolase gene family. J.A.E. and C.G.L. developed an antibody therapeutic that targets and inhibits CHI3L1 and were granted a patent to treat cancers including non–small cell lung cancer (NSCLC) and glioblastoma multiforme (GBM). It does not address nonmalignant neurologic disorders. The patent was granted to Brown University, licensed to Elkurt Inc., and then sublicensed to Ocean Biomedical (U.S. Patent No. 11,667,725; issue date: 6 June 2023; current status: active; applicant: Brown University; U.S. Patent Application No. 16/939,265; filing date: 27 July 2020; title: Methods and compositions relating to anti-CHI3L1 antibody reagents for the treatment of cancer). The other authors declare that they have no competing interests. **Data and materials availability:** All data needed to evaluate the conclusions in the paper are present in the paper and/or the Supplementary Materials. The lentiviral constructs and the transgenic mouse line other than described in this study are available from the corresponding authors with a Uniform Biological Material Transfer Agreement upon request.

Submitted 23 January 2023
Accepted 28 August 2023
Published 27 September 2023
10.1126/sciadv.adg8148